J. Fluid Mech. (1981), *vol.* 110, *pp.* 39–71
Printed in Great Britain

The 'preferred mode' of the axisymmetric jet

By A. K. M. F. HUSSAIN AND K. B. M. Q. ZAMAN
Department of Mechanical Engineering,
University of Houston, Texas 77004

(Received 27 March 1980 and in revised form 8 December 1980)

The 'preferred mode' of an incompressible axisymmetric free jet has been organized through controlled perturbation, and spatial distributions of time-average as well as phase-average flow properties in the near field are documented. The excitation produces noticeable changes in the time-average measures of the jet, although these changes are less dramatic than those for the excitation producing stable vortex pairing. For different stages in the evolution of the preferred-mode coherent structure, the phase-average vorticity, coherent Reynolds stress, and incoherent turbulence intensities and Reynolds stress have been educed through phase-locked hot-wire measurements, over the spatial extent of the structure and without invoking the Taylor hypothesis. For a particular stage of the evolution (i.e. when the structure is centred at $x/D \simeq 3$) the distributions of these quantities have been compared for both initially laminar and fully turbulent exit boundary layers, and for four jet Reynolds numbers. The relative merits of the coherent structure streamline and pseudo-stream-function patterns, as compared with phase-average velocity contours, for structure boundary identification have been discussed. The structure shape and size agree closely with those inferred from the average streamline pattern of the natural structure educed by Yule (1978).

These data as well as $\tilde{u}$-spectra show that even excitation at the preferred mode cannot sustain the initially organized large-scale coherent structure beyond eight diameters from the jet exit. The background turbulence is organized by the coherent motions in such a way that the maximum rate of decrease of the coherent vorticity occurs at the structure centres which are the saddle points of the background-turbulence Reynolds-stress distributions. The structure centres are also the locations of peak phase-average turbulence intensities. The evolving shape of the structure as it travels downstream helps explain the transverse variations of the wavelength and convection velocity across the mixing layer. The coherent structure characteristics are found to be independent of whether the initial boundary layer is laminar or turbulent, but depend somewhat on the jet Reynolds number. With increasing Reynolds number, the structure decreases in the streamwise length and increases in the radial width and becomes relatively more energetic, and more efficient in the production of coherent Reynolds stress.

1. Introduction

Recent theoretical and experimental investigations in axisymmetric jets have established that there exists a preferred frequency at which an axisymmetric disturbance receives maximum amplification in the jet column. With the help of flow visualization and hot-wire measurements in a sinusoidally perturbed jet, Crow & Champagne (1971) showed that this 'preferred mode' corresponded to a Strouhal number $St_D = f_p D/U_e$ of about 0·30, where f_p is the excitation frequency, D is the jet diameter and U_e is the jet exit speed. Essentially the same St_D value of the 'preferred mode' has also been confirmed by us in several jets with a variety of initial conditions, although it has been found to increase somewhat at lower Reynolds numbers.† These results together with investigations of controlled perturbation of the axisymmetric jet involving stable vortex pairing, have been summarized by Zaman & Hussain (1980, hereinafter referred to as I).

The circular jet preferred mode is independent of the exit shear-layer instability characteristics, because the characteristic length scale of the mode has been shown to be the jet diameter and not the width of the exit shear layer. This inference is further supported by the fact that the preferred-mode Strouhal number, as identified by the maximum amplification of centre-line velocity fluctuation, has been shown in I to be the same, irrespective of the exit boundary layer being laminar or fully turbulent.

The significance of the preferred mode lies in the fact that it is the most dominant and frequently occurring of all large-scale coherent structures in an unperturbed circular jet. Crow & Champagne (1971) demonstrated this by flow-visualization experiments, in which 'vortex puffs' in the near field of an unperturbed circular jet formed at a modal frequency of $St_D \simeq 0{\cdot}30$. Browand & Laufer (1975) showed by flow visualization in a low Re_D (5000–15000) water jet that the natural structures at the end of the potential core had the passage frequency of $St_D = 0{\cdot}5$; also, this is consistent with our observation that the St_D value for the preferred mode increases somewhat with decreasing Re_D.

An incompressible shear flow is a function of the initial condition, the boundary condition and the Reynolds number. Provided that the Reynolds number is sufficiently high and the flow domain is very large compared with the width of the shear flow, the evolving free flow is a function only of the initial condition. When initially laminar, the shear layer rolls up at frequencies within the unstable band and undergoes successive interactions like pairing and tearing through which the flow achieves gradual independence from the initial condition. An initially fully turbulent shear layer can also roll up and undergo successive interactions. While this can continue indefinitely in a plane mixing layer, these initial structures tend to evolve to a 'terminal structure' in the near field of a circular jet by about 2–3 diameters where the structure characteristics scale on the jet diameter and should be essentially independent of the initial condition. (It is not suggested that this 'terminal structure' persists in the self-preserving region of a jet. The existence of large-scale coherent structures in the self-preserving region of the jet is still an open question and is being investigated in our laboratory.) Therefore, an unperturbed circular jet contains a 'latent orderly structure' near the end of the potential core corresponding to $St_D \simeq 0{\cdot}3$.

† In fact, the St_D value for the apparent 'preferred mode' found by several other investigators fall in a range; for example: 0·35 by Moore (1977), 0·35 by Chan (1974), 0·48 by Bechert & Pfizenmaier (1975) and 0·5 by Vlasov & Ginevskiy (1974).

It is necessary to emphasize here that no jet flow is truly 'unperturbed', as each flow is exposed to disturbances originating from a variety of effects including rotating stall, blade wake, tunnel cavity resonance, standing acoustic waves in the laboratory, disturbances from flow impingement and obstructions downstream, shear tones inside and outside the tunnel, etc. as well as some random disturbances. These together manifest themselves as the 'free-stream turbulence'. If any one of the background disturbance modes is predominant (say, appearing as a clear, large-amplitude spike in the spectrum of the free-stream turbulence), the jet would tend to lock onto it and roll up at this frequency provided that it is in the unstable band. In all such cases, the jet can be considered as 'driven'. In the case of a 'white-noise'-like background disturbance, however, the large-scale structures in the 'unperturbed' jet would most frequently occur at the preferred-mode frequency (i.e. $St_D \simeq 0{\cdot}3$), though randomly and in combination with structures of other frequencies and sizes. Controlled excitation at $St_D \simeq 0{\cdot}3$ organizes the (natural) preferred-mode structures to form at regular intervals, i.e. at controlled phases, as well as eliminating formation of structures at other frequencies. Because of the organization of the structures via elimination of the otherwise inherent jitter and of the structures at other frequencies, the time-average measures of the jet are expected to be modified from those of the corresponding unexcited state; however, the coherent structure under excitation at $St_D \simeq 0{\cdot}3$ should be the same as the 'preferred-mode' coherent structure of the unexcited jet.

The relevance of the natural structures to the excitation-induced structures is a valid inquiry. It should be recognized that excitation at any arbitrary frequency may produce a structure which may be infrequent in the natural flow, especially if the excitation is of a large amplitude. In that case, the relevance of the excited structure can indeed be questionable, even though such a study may be of some technological interest. In the present case of controlled perturbation at the preferred mode, the relevance should be readily recognized since a detailed study of the most dominant natural structure is merely facilitated by the excitation which provides unambiguous phase reference.

The primary motivation for the controlled excitation is that it greatly simplifies the coherent structure eduction. The periodic passage of the structure, especially nearer the structure-formation region, permits eduction of the structure details through the comparatively much easier method of phase averaging by using the excitation period for phase lock. It should be emphasized that, even if it were possible to isolate the preferred-mode coherent structure from other structures in an unperturbed jet, their dispersion in shape, size, orientation, strength, convection velocity, etc. would frustrate any attempt to obtain their characteristics through ensemble averaging (Bruun 1977; Yule 1978). Controlled excitation, through phase information, enables eduction of structure properties to such details and accuracy that are not likely to be possible even with highly sophisticated eduction schemes in an unperturbed flow. Thus, although the dispersions in shape, size, etc. of the structures are integral aspects of turbulence, controlled excitation appears to be unavoidable, even the only viable approach, for the eduction of the structure properties.

The present study was motivated by the fact that although the maximum amplification of an axisymmetric disturbance, as denoted by the longitudinal intensity on the jet centre-line, has been found to occur at $St_D \simeq 0{\cdot}3$, no effort has been devoted in the past to explore the characteristics of the corresponding large-scale coherent

structure. Also unknown is the possible dependence of the features of the preferred-mode coherent structure on the Reynolds number and the initial condition. This study documents the detailed characteristics of the preferred-mode coherent structure and its evolution as well as the effect of the organization on the time-average measures of the jet near-field. Phase-average spatial distributions of different properties have been obtained over the extent of the structure cross-section at desired phases (see Hussain & Reynolds 1970 and Hussain & Zaman 1980 for discussions of the associated concepts). These phase-average data, obtained by repeating the measurements at different spatial points over the extent of the coherent structure, do not invoke the Taylor hypothesis as done in almost all other investigations of coherent structures (for example, Wygnanski, Sokolov & Friedman 1976; Zilberman, Wygnanski & Kaplan 1977; Cantwell *et al.* 1978; Browand & Wiedman 1976; Sokolov *et al.* 1980) and thus represent the *actual* distributions of the flow properties over the spatial extent of a structure. The phase-average spatial details, e.g. vorticity and Reynolds stresses, are then examined in order to obtain some understanding of the preferred-mode coherent structure dynamics and its dependence on the initial condition and the jet Reynolds number.

Since coherent structures appear to be inherent to all turbulent shear flows, it is clear that any realistic turbulence theory must incorporate these structures directly. That is, newer theories must be built with the coherent structures as the building blocks. Thus, in addition to understanding the dynamics of coherent structures, a major motivation for this study was to document the heretofore unavailable coherent structure properties which would be necessary for development of a viable turbulence theory. Furthermore, the detailed time-average measures of the unexcited and excited jets presented here are quite likely to find use both in technological applications and in evaluation of prediction codes. In particular, the controlled excitation data should serve as critical calibrators of both time-independent and time-dependent codes.

2. Experimental procedures

The experiments were carried out in a circular air jet described in I. Most of the data presented are for a 7·62 cm diameter nozzle at the Reynolds number $Re_D = 55000$. A thin sandpaper ring tripped the boundary layer at 4 cm upstream from the nozzle exit. The exit boundary layer was inferred to be fully-developed turbulent on the basis of the mean velocity and longitudinal fluctuation intensity profiles and $\tilde{u}$-spectra (see table 1; for further details see I). The mean velocity profile, consisting of distinct logarithmic and wake regions in universal (u^+, y^+) co-ordinates, closely agreed with the flat-plate equilibrium boundary layer and had a shape factor of about 1·4. The longitudinal fluctuation intensity increased monotonically from the free-stream value of 0·28 % to its maximum at $y^+ \simeq 13$, and had a broadband spectrum ϕ_u extending up to about 8 kHz without any sharp peak. The untripped-boundary-layer profile agreed with the Blasius profile with a fluctuation-intensity profile peaking at $y/\delta^* \simeq 1$, typical of laminar boundary layers; δ^* is the displacement thickness of the boundary layer. The controlled excitation at the nozzle exit was induced by means of a loud-speaker attached to the first settling chamber of the two-chamber jet facility (for details, see I). This study was carried out at an excitation amplitude (u'_e/U_e) of 2 %, measured at the jet exit centre-line. This excitation did not produce any change in

Nozzle	$Re_D \times 10^{-3}$	f_p (Hz)	Exit boundary-layer characteristics: θ (cm)	δ_1/θ	u'_{max}/U_e
7·62 cm tripped	55	44	0·0343	1·56	0·114
7·62 cm untripped	55	44	0·0203	2·60	0·010
7·62 cm tripped	110	87	0·0511	1·60	0·105
2·54 cm tripped	25	178	0·0432	1·73	0·123
2·54 cm tripped	44	312	0·0480	1·49	0·093

TABLE 1. Initial conditions.

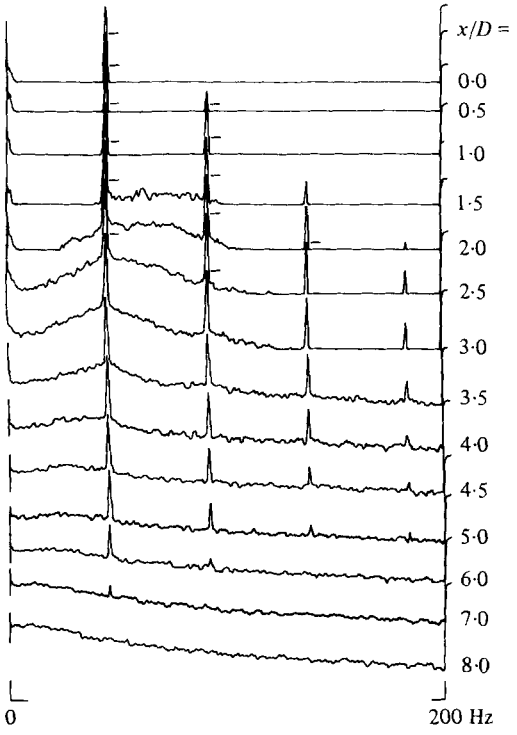

FIGURE 1. $\tilde{u}$-spectra at different x on the centre-line of the 7·62 cm (tripped) jet, excited at $St_D = 0{\cdot}30$ ($f_p = 44$ Hz), $u'_e/U_e = 2\,\%$, $Re_D = 55\,000$ ($U_e = 10{\cdot}8$ m s^{-1}).

the exit mean velocity profile for either initial condition. An analog (DISA) turbulence processor was used to obtain the instantaneous $\tilde{u}(t)$ and $\tilde{v}(t)$ signals from an X-wire (4 μm diameter tungsten), operated at an overheat ratio of 0·4 by linearized DISA constant-temperature anemometers. Mean and r.m.s. fluctuation velocities were found to be axisymmetric in the near field. Data were acquired on a horizontal diametral plane on one side of the jet centre-line, in the measurement region extending over $0 \lesssim x/D \lesssim 14$. At each spatial point, time-average and phase-average quantities were computed on-line with a laboratory minicomputer (HP2100). Probe traverse was performed via a precision, backlash-free traversing mechanism under computer control. Further details of the measurement procedures including phase-averaging,

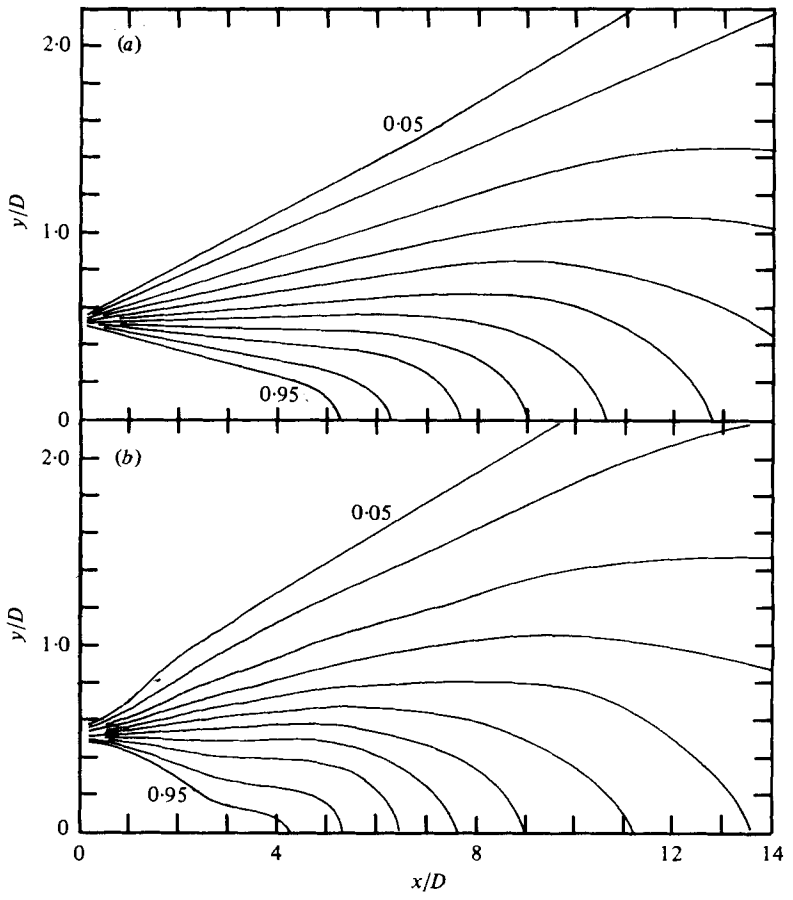

FIGURE 2. Contours of U/U_e for the flow in figure 1 : (*a*) without excitation, (*b*) with the excitation. Contour levels in sequence are 0·05, 0·1, 0·2, 0·3, 0·4, 0·5, 0·6, 0·7, 0·8, 0·9, 0·95.

triggering technique, data acquisition and analysis have been discussed by Hussain & Zaman (1980; hereinafter referred to as II).

3. Results and discussion

3.1. *Time-average data*

Data in figures 1–15 pertain to the 7·62 cm diameter tripped jet at $Re_D = 55000$; the frequency f_p for the excitation cases was 44 Hz. Figures 16–18 include data for a 2·54 cm jet as well. These data for different Reynolds numbers and initial conditions involve excitation at frequencies such that the St_D is 0·30 in all cases.

Figure 1 shows the centre-line evolution of the spectra of the longitudinal velocity, $\tilde{u}(t)$; all the traces have the same logarithmic ordinate and linear abscissa scales. These spectra, representing averages over 64 realizations, were obtained with a real-time spectrum analyser with a resolution of 500 lines (Spectrascope SD335). The spectral peak at the fundamental (i.e. at the driving frequency $f_p = 44$ Hz) grows to a maximum at $x/D \simeq 3{\cdot}5$, and then decays until submerged in the evolving turbulence at $x/D \simeq 8$, beyond which the spectrum is fully developed and is free from any peak.

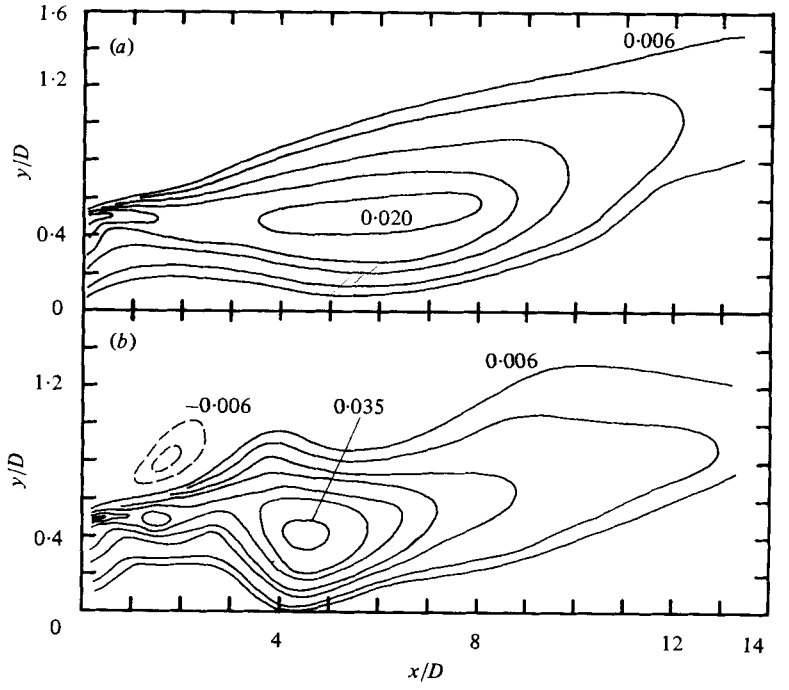

FIGURE 3. Contours of V/U_e for the flow in figure 1: (*a*) without excitation, (*b*) with the excitation. Contour levels in sequence are −0·006, −0·010, 0·006, 0·008, 0·012, 0·015, 0·020, 0·025, 0·035.

Generation of the higher harmonics begins from $x/D \simeq 0{\cdot}5$. The absence of any subharmonic peak, anywhere in x, suggests that the preferred-mode structures convect downstream as a single street without any pairing; the direct correspondence between a subharmonic peak and vortex pairing has been discussed in I.

Spatial distributions of time-average flow properties in an azimuthal plane (passing through the jet axis) are documented in figures 2–6 as constant level contours; in each figure, data for the unexcited jet are shown in (*a*), while the corresponding data for the excitation case are shown in (*b*).

The contours of the longitudinal mean velocity in figures 2(*a*, *b*) show that excitation produces a relative widening of the shear layer (and hence of the jet) and a shortening of the potential core. Note that the linear spread of the axisymmetric shear layer in the unperturbed case is noticeably distorted by the excitation. The contours of the time-average transverse mean velocity V for the unexcited jet (figure 3*a*) exhibit a maximum value of $0{\cdot}02U_e$ near the shear layer in the range $3{\cdot}5 \lesssim x/D \lesssim 8$, the region of disintegration of the toroidal structures (near the end of the potential core). For the excitation case, this region of interaction shifts upstream and becomes more localized and intensified (figure 3*b*). The negative V region in figure 3(*b*) indicates mean inward flow, associated with the regularized roll-up of the turbulent shear layer under excitation (to be discussed later with phase-average vorticity data). The peak positive value of V is now $0{\cdot}035U_e$ and occurs at $x/D \simeq 4{\cdot}5$.

Figures 4(*a*, *b*) show that the longitudinal turbulence intensity u'/U_e whose streamwise distribution on the centre-line has one peak (at $x/D \simeq 8{\cdot}5$) develops two peaks (at $x/D \simeq 3$ and 7) when excited. The axial locations of the two peaks (figure 4*b*)

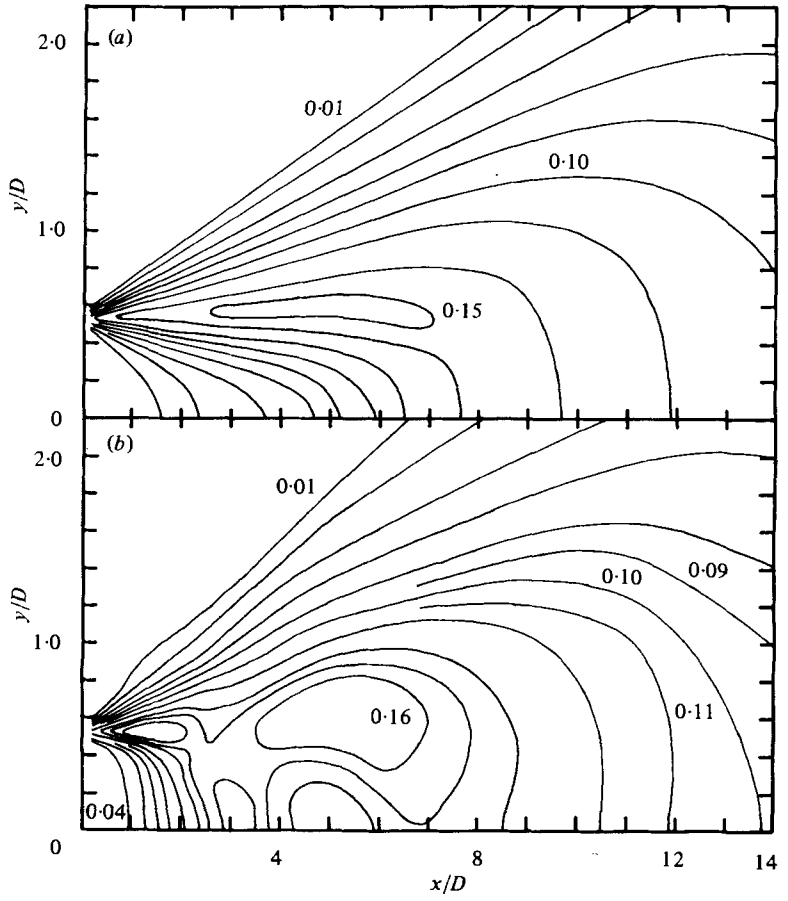

FIGURE 4. Contours of u'/U_e for the flow in figure 1: (*a*) without excitation, (*b*) with the excitation. The unmarked contour levels in sequence are 0·02, 0·04, 0·06, 0·08, 0·12, 0·14, 0·15.

shift upstream as one moves away from the centre-line, occurring at $x/D \cong 1{\cdot}5$ and 5 in the shear layer. The first peak in the $u'(x)$ variation can be attributed to the roll-up of the turbulent shear layer into the preferred-mode structure (see later). The second peak in the $u'(x)$ variation is believed to be associated with the breakdown of the initial toroidal structure at the end of the potential core (see I; Zaman & Hussain 1981). The excitation-induced modification of the turbulence structure is most significant within about the first 5 diameters from exit. For $x/D \gtrsim 8$, there is no dramatic difference between the u' contours for the excited and unexcited cases.

The $v'(x)$ data exhibit single peak variation all across the jet, for both the unexcited and excited cases (figures 5*a*, *b*). Most dramatic modification of the v' distribution by excitation also occurs approximately within the first five diameters; the differences farther downstream between the excited and unexcited cases are not remarkable except that the location of the peak on the centre-line moves upstream from $x/D \simeq 9{\cdot}5$ to 7. Note that, while excitation does not noticeably alter the peak u'-levels in the shear layer, the peak v'-levels are increased from a smooth peak region to a sharp ridge, the peak value having increased by about 50 %.

Figures 6(*a*, *b*) show that the excitation localizes Reynolds stress and increases the

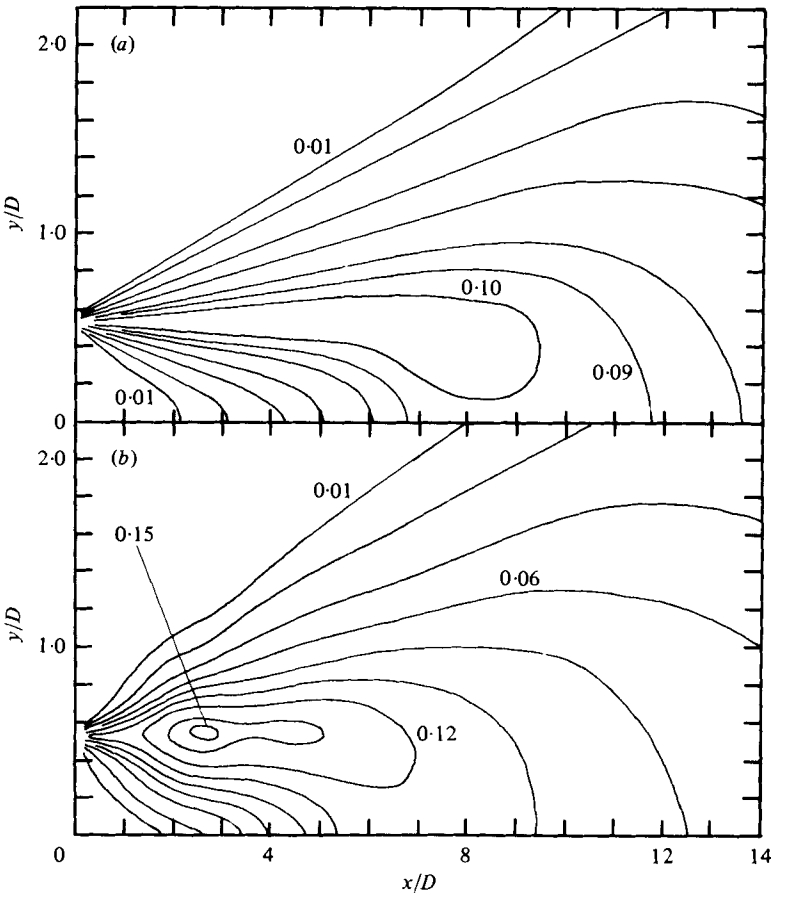

FIGURE 5. Contours of v'/U_e for the flow in figure 1: (*a*) without excitation, (*b*) with the excitation. Contour levels in sequence are 0·01, 0·02, 0·04, 0·06, 0·08, 0·10, 0·12, 0·14, 0·15.

peak value by about 50 %. Of the U, V, u', v', $\overline{uv}$ data for either the excited or the unexcited case, the width of the $u'(y)$ profile is the largest and of the $\overline{uv}(y)$ profile the smallest. Excitation at the preferred mode produces noticeable widening of all the profiles. These modifications of the time-average property distributions due to excitation at $St_D = 0{\cdot}30$ are not unexpected. The preferred-mode excitation does not induce any artificial structures, but only organizes the formation of the most dominant of all natural structures. While the time-average property distribution in the unexcited jet is the average imprint of a variety of natural structures with large dispersion in shape, size, orientation, strength, etc. as well as their interactions, the distributions for the present excited case is due only to the preferred-mode structure. However, since the preferred-mode structure does not undergo pairing and, since it is the most dominant of all natural structures, the modifications brought about in the time-average distributions are not as dramatic as in the case of excitation inducing stable pairing. Excitation in the latter case increases $\overline{uv}$-peaks by as much as 200 %, as well as producing significant regions of negative Reynolds stress. For the magnitudes and locations of negative $\overline{uv}$, as well as other changes brought about by excitation inducing stable pairing, see I.

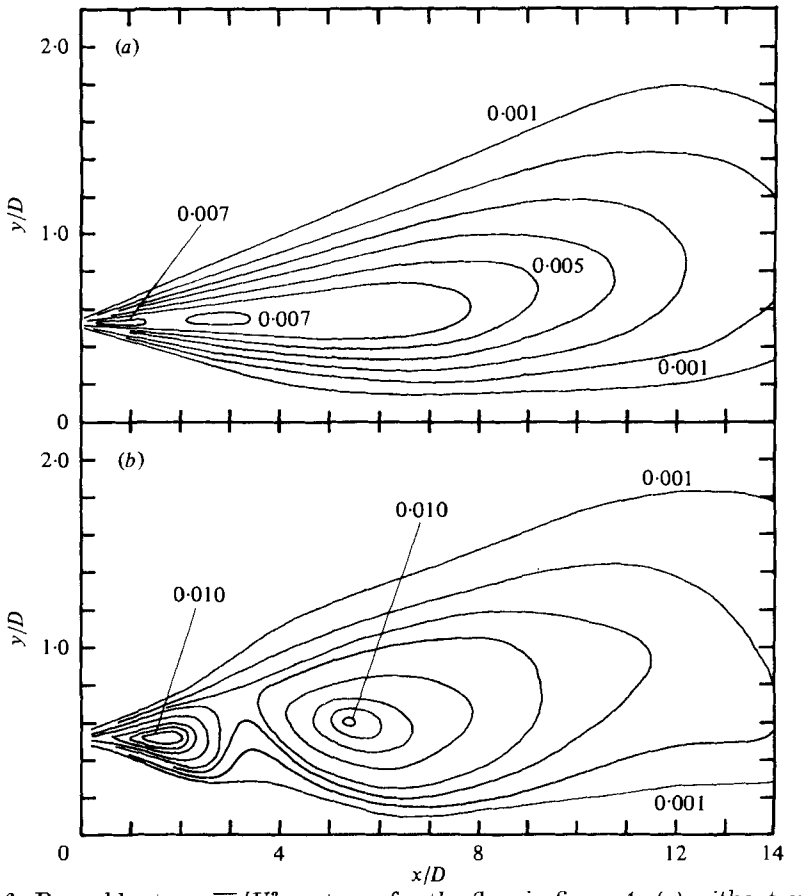

FIGURE 6. Reynolds stress $\overline{uv}/U_e^2$ contours for the flow in figure 1: (*a*) without excitation, (*b*) with the excitation. The unmarked contour levels are in the sequence 0·002, 0·003, 0·004, 0·006, 0·008, 0·009.

3.2. *Preferred-mode coherent structure*

The time-average 'footprints' of the preferred-mode coherent structure, discussed above, do not reveal the details of the structures themselves which are presumed to be at the heart of transport and noise production mechanisms in the near field of the circular jet. It was thus considered both interesting and worthwhile to educe the instantaneous (i.e. phase-average) spatial details of these structures in the jet.

Throughout this paper, we shall use the decomposition: $\tilde{g} = \langle g \rangle + g_r, \langle g \rangle = G + \langle g_p \rangle$; where $\tilde{g}$ is the instantaneous value of a function, G is its time mean, $\langle g_p \rangle$ is the periodic component of the phase average, and g_r is the component due to the background turbulence field. The phase-average r.m.s. of the last is defined as

$$\langle g_r^2 \rangle^{\frac{1}{2}} = \left[\lim_{N \to \infty} \frac{1}{N} \sum_{n=1}^{N} g_r^2(t + n\tau) \right]^{\frac{1}{2}},$$

where τ is the period between successive structures.

Contours of phase-average properties over the spatial extent of the coherent structure were measured on-line with the laboratory minicomputer system. The measurement technique essentially amounted to freezing the structure at a particular phase (in a spatial measurement region) and obtaining data with an X-wire at different spatial locations over the extent of the structure at that phase. This was carried out

by detecting the passage of a structure at a particular location with a reference probe and using a feature of the reference signal to trigger the sampling of the X-wire voltages by the computer.

The phase for each measurement region was chosen as follows. The reference wire was placed on the jet centre-line at the location x_M at which the structure to be educed was expected to be centred. From the reference signal, a triggering signal was derived via a bandpass filter and a triggering device. The triggering signal (periodic at frequency f_p) and the reference signal $u(t)$ were displayed simultaneously on a dual-beam oscilloscope. The high voltage dwell of the triggering signal was then set (through a potentiometer in the triggering device) such that the instants of voltage drops approximately corresponded to the peaks in the periodic $\tilde{u}(t)$ signal. The computer sampled data from the X-wire at the instants the triggering signal dropped from the high to the low levels. For a given location (x, y) of the X-wire, an average over a large ensemble (typically 3000) of data obtained at successive triggers gave the phase-average measures. Note that the chosen phase was such that the phase-average $\langle u\rangle(x)$ should have a peak at $x \simeq x_M$ on the centre-line. Keeping the trigger setting unaltered, the X-probe was then moved to different grid points in a particular measurement region for on-line computation of $\langle u\rangle$, $\langle v\rangle$ as well as $\langle u_r^2\rangle^{\frac{1}{2}}$, $\langle v_r^2\rangle^{\frac{1}{2}}$, $\langle u_r v_r\rangle$ as functions of (x, y). Further details of the measurement procedures have been described in II.

Contours of phase-average vorticity ($\Omega_z = \partial\langle v\rangle/\partial x - \partial\langle u\rangle/\partial y$) for eight successive phases in the evolution of the coherent structure in the shear layer are shown in figures 7 (*a*)–(*h*). These vorticity data, non-dimensionalized by the excitation frequency f_p, were computed from the measured spatial distributions $\langle u\rangle(x, y)$ and $\langle v\rangle(x, y)$ at the selected phases as discussed above.

Recognizing that the peak in the $\tilde{u}(t)$ signal occurs when a structure is passing through a transverse plane at $x \cong x_M$, the above choice of the phase should result in an educed structure centred at $x \simeq x_M$. This phase selection, for the eight regions in figures 7 (*a*)–(*h*), was done so that the captured vortex centres would be located at $x_M/D = 1$, 1·5, 2, 2·5, 3, 4, 5, 6 and 8, respectively. Note that at $x_M/D = 6$ and 8, the $\tilde{u}(t)$ signal on the jet centre-line had too much large-amplitude random fluctuations to permit its use as a reference signal for unambiguously triggering data sampling. In these regions, the 'wavelength' information was used, and the phase setting was done with the reference signal derived from a location one 'wavelength' upstream from the desired x_M. As mentioned earlier, the reference probe (used to obtain the triggering signal) was located near the jet centre-line at the corresponding x_M. This choice is immaterial for a truly periodic underlying waveform in the velocity signal, but was motivated by the hope of minimizing the triggering signal jitter relative to the vortex arrival time, especially at larger x/D values.

It is interesting that the eduction process has been successful in sifting out, from the large-amplitude random velocity signals, not only the preferred-mode coherent structure but also its streamwise evolution. More impressive is the fact that these contours show the roll-up of an initially turbulent shear layer into the jet-column preferred-mode structure.

The roll-up process for the flow situation under study is captured in figures 7 (*a–c*). At the onset of the roll-up at $x/D \simeq 1{\cdot}5$, the rise and fall in $\tilde{u}(t)$ (and hence in $\langle u\rangle(t)$) are associated with characteristic tilt in the structure as revealed by the vorticity

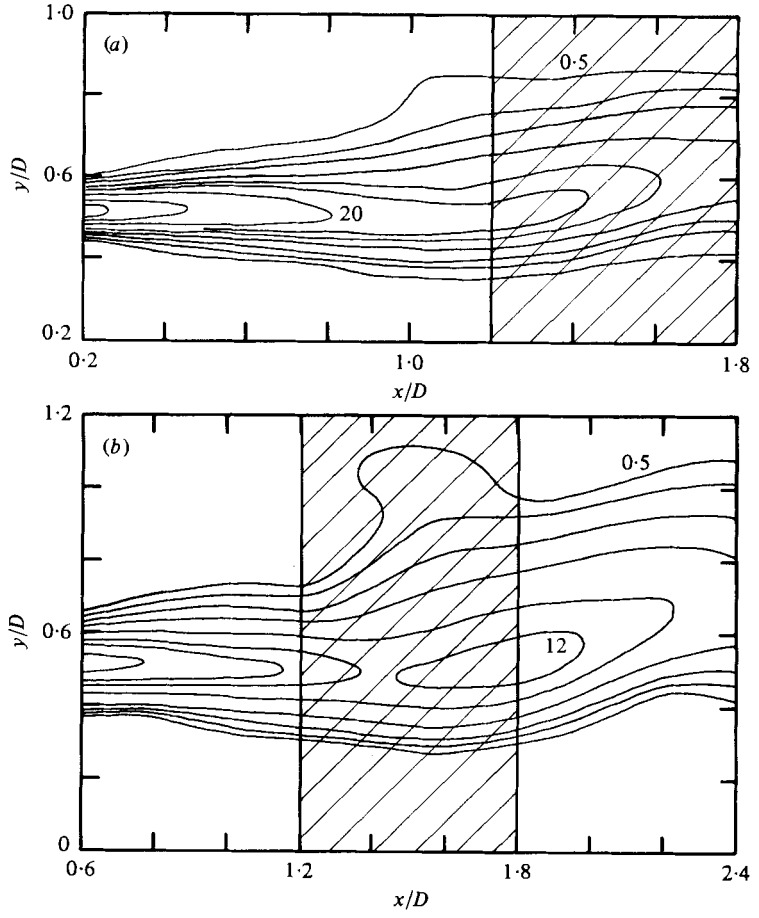

FIGURE 7. Contours of phase-average vorticity Ω_z/f_p at different phases of the structure evolution, for the flow in figure 1. The contour levels in sequence are: (*a*) 0·5, 2, 4, 8, 12, 15, 20, 30, 40; (*b*) 0·5, 1, 2, 4, 8, 12, 20; (*c*) 0·5, 1, 2, 4, 6, 8, 10, 12; (*d*) 0·5, 1, 1·5, 2, 2·5, 3, 4, 5, 6, 8, 10; (*e*) 0·5, 1, 1·5, 2, 3, 4, 5, 6, 7; (*f*) 0·5, 1, 1·5, 2, 2·5, 3, 3·5, 4, 5; (*g*) 0·5, 1, 1·5, 1·8, 2, 2·5, 3, 3·3, 3·5; (*h*) 0·5, 0·8, 1, 1·2, 1·4, 1·7, 2, 2·4, 2·7.

contours. Consider, for example, the (shaded) region $1{\cdot}2 < x/D < 1{\cdot}8$, in figures 7 (*a–c*). By choosing the phase as discussed earlier, a probe placed at $x/D = 1{\cdot}5$ on the jet centre-line would sense a maximum $\langle u \rangle(t)$ at the phase (or time t) corresponding to that of figure 7 (*b*). The vorticity contours in figure 7 (*b*) within the x-range under consideration are found to be approximately parallel to the x-axis near the jet centre-line. Figure 7 (*c*) represents the structure at a slightly later phase (or time), and the forward tilt of the vorticity contours (i.e. forward end leaning towards the jet centre-line) corresponds to an increasing velocity of the fluid on the centre-line with increasing x. Similarly, the characteristic tilt in the opposite way in figure 7 (*a*) corresponds to a decreasing velocity on the centre-line with increasing x. At farther upstream locations, say at $x/D \simeq 0{\cdot}6$ in figures 7 (*a*, *b*), no significant tilting of the vorticity contours is apparent, and the periodic velocity fluctuation should be associated with a 'vorticity wave', i.e. passage of alternate concentration and reduction of vorticity sensed by a probe at a fixed point in the shear layer.

At the downstream stations, the vortex cross-sections are somewhat tilted with the

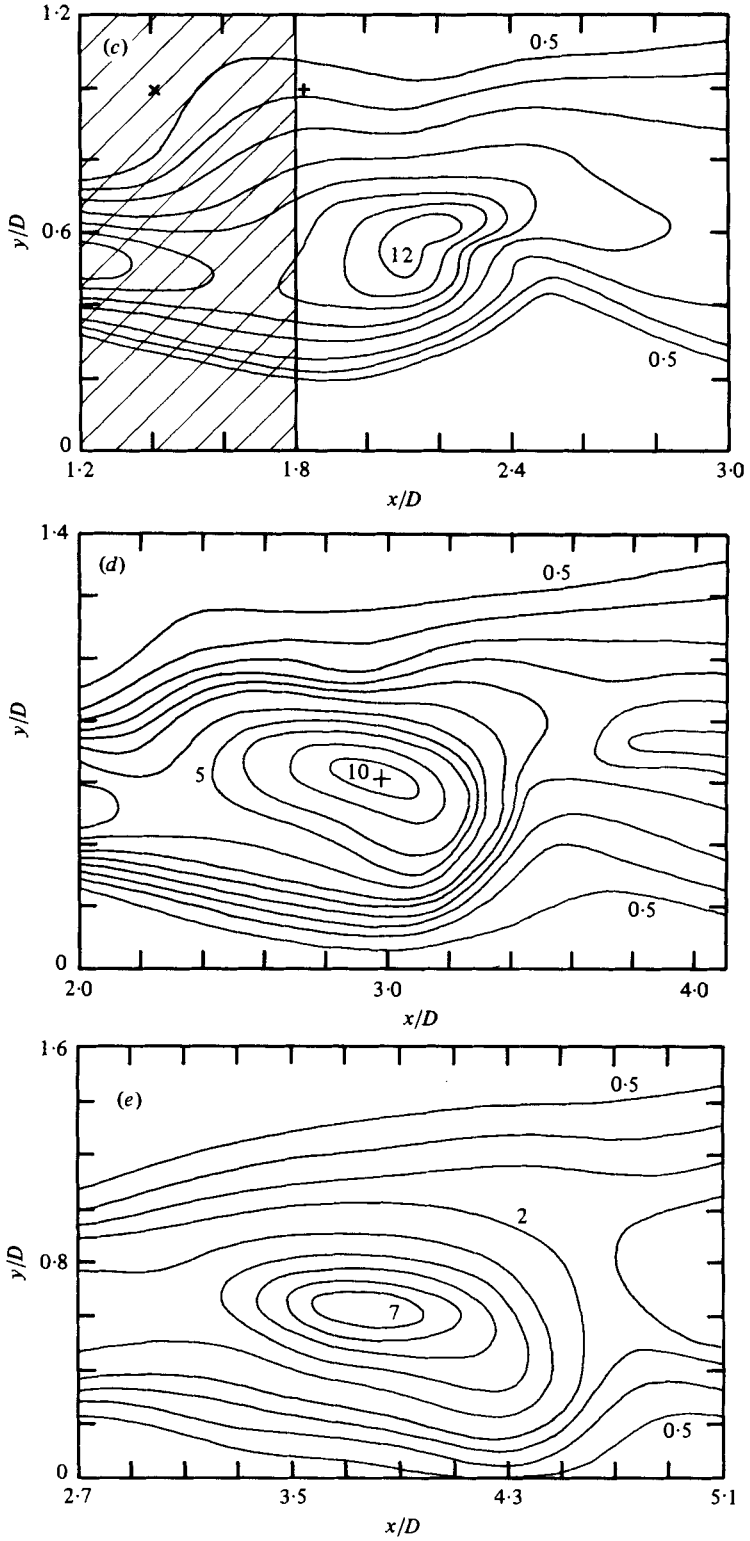

FIGURE 7(*c*, *d*, *e*). For legend see p. 50.

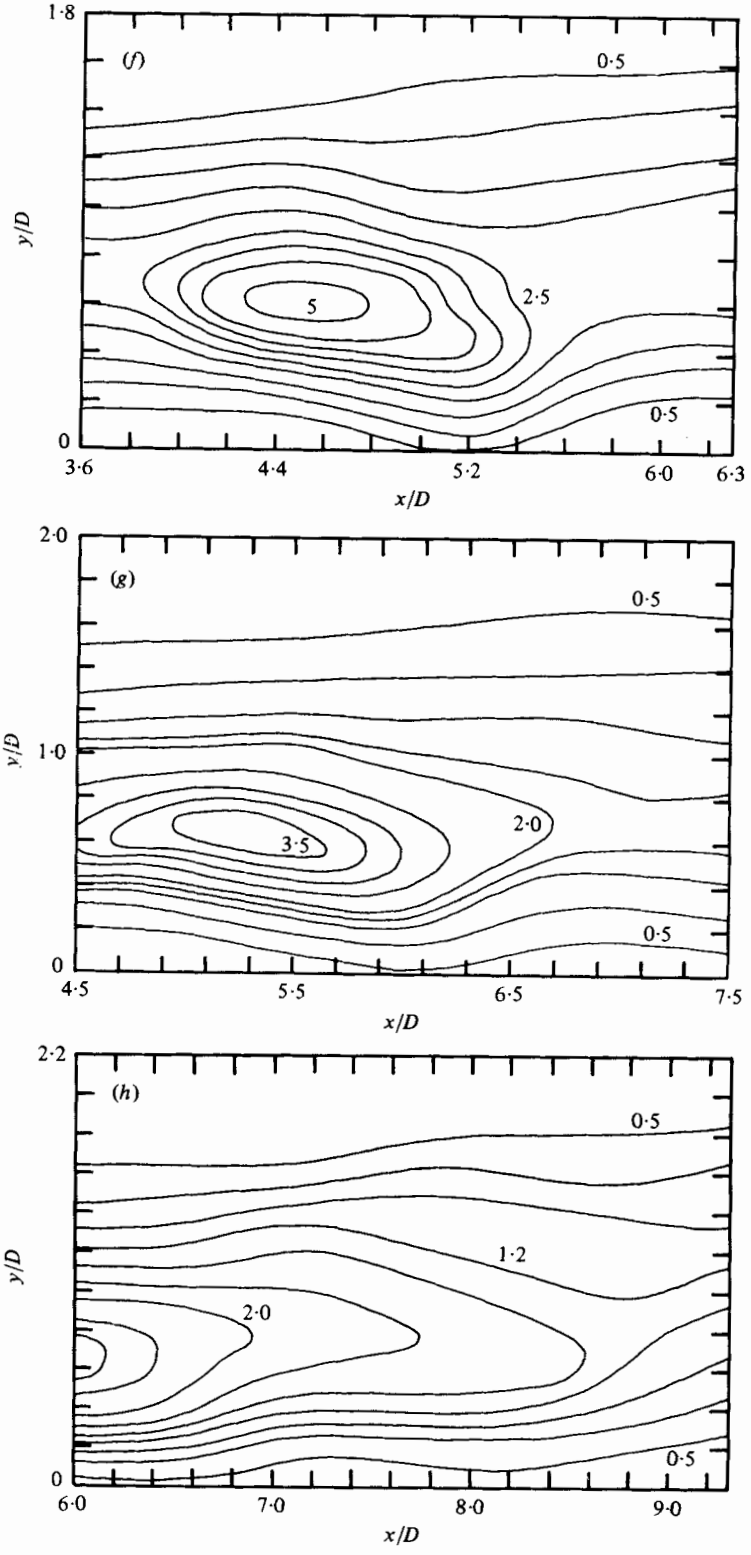

FIGURE 7(*f*, *g*, *h*). For legend see p. 50.

front ends leaning towards the jet centre-line (e.g. in figure 7*e*). Considering the evolution of the cross-section of the vortical structures, e.g. between the phases corresponding to figures 7(*c*) and 7(*e*), it is clear that the apparent tilting of the vortex is a direct consequence of shear across the vortex cross-section: that is, the high-speed side of the structure moving faster relative to the structure centre. Especially, the fairly rapid development of the kink in the contour between figures 7(*b*) and 7(*c*) is a result of this acceleration of the high-speed side of the vortex.

As a result of the tilting of the vortex, the peak in the periodic $\tilde{u}(t)$ signal measured on the centre-line occurs at a time earlier than that when the corresponding vortex centre arrives at the same axial station. This explains why the vortex centre in a downstream region occurred somewhat upstream from its estimated axial location x_M. For example, while the vortex centre was estimated from the centre-line $\tilde{u}(t)$ signal to be located at $x_M/D \simeq 5$, the actual location is found to be at $x/D \simeq 4{\cdot}5$ (figure 7*f*).

(*a*) *Explanation of some time-average data trends.* The roll-up process is marked by a sudden widening of the shear layer and appearance of a pronounced 'hump' in the vorticity contours on the low-speed side (figures 7*a–d*). Consider a point upstream of this hump in figure 7(*c*), marked by a $\times$. Assuming that the constant vorticity contours closely represent the streaklines in the flow (Michalke 1972; II), the transverse velocity at this point and at the phase under consideration should be negative. On the other hand, on the downstream side of the hump, e.g. at the point marked by the $+$, where the vorticity contours are essentially parallel to the x axis, the transverse velocity should be nearly zero. Thus, on the low-speed side, and in the range $1 \lesssim x/D \lesssim 2{\cdot}5$ where the roll-up of the vortex is completed, the phase-average transverse velocity at different phases is either negative or zero. This should account for the negative time-average V in this region (figure 3*b*).

The first peak of u' in figure 4(*b*), in the middle of the shear layer, is found to occur at about $x/D = 1{\cdot}5$. This is roughly the location of initiation of the shear-layer roll-up (see figures 7*a–c*). At this axial station, however, the signature of the rolled-up vortices is relatively weak on the centre-line because of the smaller cross-section of the vortices and thus u' is found to be small on the centre-line. The roll-up process is essentially complete at $x/D \simeq 2$. From this location downstream, while the structure core peak vorticity gradually drops, the core size significantly enlarges. The centre-line velocity fluctuation sensed by a stationary probe is due to the induced velocity of the vortical structure in the outside potential flow (decreasing as r^{-1} if r is the distance from the structure centre). The induced velocity on the jet centre-line is augmented owing to the axisymmetric configuration and also, presumably, the acceleration of the jet core fluid as it moves through the interior of the toroidal structure. Thus, even though the structure core vorticity level gradually drops with increasing x, the increasing size of the vortices results in increasingly stronger 'footprint' on the jet centre-line and thus larger fluctuation intensities. The longitudinal fluctuation intensity reaches a maximum at $x/D \simeq 3$ presumably because the centre-line 'footprint' of the structure becomes the strongest at this station, before beginning to weaken. At $x/D \gtrsim 5$, the level of the vorticity in the cores of the vortices (see figures 7*f*, *g*) has dropped significantly so that the weak and diffuse structure itself has a weak induced velocity outside as well as offering no significant resistance to the core flow for the latter to accelerate. This should thus explain the first peak in $u'(x)$ and also why it occurs at a larger x on the centre-line than in the shear layer.

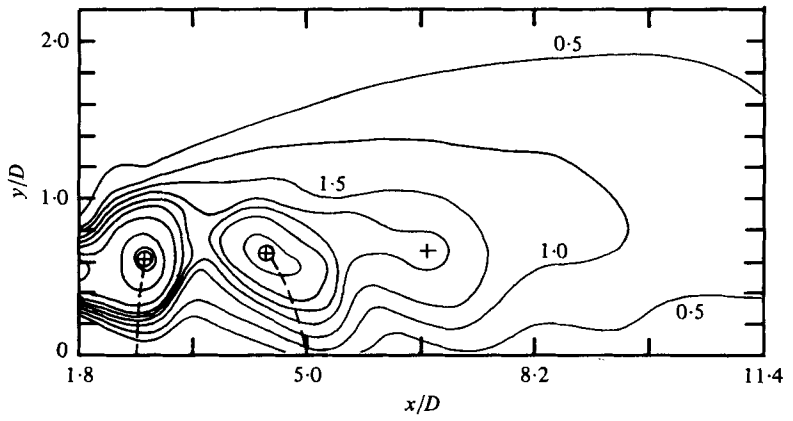

FIGURE 8. Contours of phase-average vorticity Ω_z/f_p for one phase over $1{\cdot}8 \leqslant x/D \leqslant 11{\cdot}4$, for the flow in figure 1. The contour levels in sequence are 0·5, 1, 1·5, 2, 2·5, 3, 4, 6, 8.

(*b*) *Loss of periodicity in the structure passage.* With increasing downstream distances from $x/D \simeq 4$, the core size of the educed structure progressively diminishes, but, beyond $x_M \simeq 8D$, closed vorticity contours are totally absent (figure 7*h*). Figure 8 shows constant vorticity contours for one particular phase over a large axial range, namely $1{\cdot}8 \leqslant x/D \leqslant 11{\cdot}4$. For these data, the reference probe for the triggering signal was located at $x/D = 5$ on the jet centre-line. In addition to the coherent structures at $x/D \simeq 2{\cdot}8$ and 4·6, there appears an apparent remnant of a vortical structure centred at $x/D \simeq 6{\cdot}6$. But farther downstream, the phase-average measurements do not reveal any structure. This can be due to a number of possible situations. First, a breakdown and randomization of the coherent vortices at this downstream location; that is, the initially (induced) large-scale structure may disintegrate before this station is reached. A second possibility is that the initial toroidal structure develops azimuthal lobes, and then divides into coherent substructures (see II). Since these substructures have no azimuthal reference, successive substructures would have random spanwise locations. There is a third possibility that the jitter between successive structures is large. The effect of the latter two would be to smear out the educed property contours even when distinct structures actually exist in the flow. It is quite likely that the reality is a combination of all the three possibilities. (Note that a periodic undulation in the $\Omega_z/f_p = 0{\cdot}5$ contour, on the high-speed side, persists farther downstream, indicating the possible remnants of the periodic coherent structure.) However, one can at least infer from these data that, even though the coherent structures are initially organized by excitation at the preferred mode, the periodicity in their passage is practically lost beyond $x/D \simeq 8$ (see also figure 1).

(*c*) *Structure spacing and convection velocity.* As discussed earlier, it should be clear that $\langle u \rangle(x)$, on the high-speed side of the shear layer, should be maximum at a point where the vorticity contour has an inward bulge and where the tangent to the vorticity contour is approximately parallel to the x axis. This has been checked by comparing contour plots of either $\langle u \rangle$ or $\langle u_p \rangle$ (not shown) with the vorticity contours. Thus, the periodic component in the $\tilde{u}$-signal, measured on the jet centre-line corresponding to the phase in figure 8, have maxima at $x/D \simeq 2{\cdot}6$, 5·0 and 7·2. On this basis, the wavelength measured on the jet centre-line would be about $2{\cdot}4D$ in the first 5 diameters

and about $2{\cdot}2D$ farther downstream. The wavelength $2{\cdot}4D$ within the potential core agrees with that measured by Crow & Champagne (1971) on the basis of comparison of $\tilde{u}$-signals on the jet centre-line. However, this value is far different from the actual centre-to-centre spacing of the vortices, which is found to be $1{\cdot}75D$ in figure 8. (The locations of the centres of the two upstream structures are marked by the symbol $\oplus$, while a 'plus' symbol denotes the centre of the residual structure at $x/D \simeq 6{\cdot}6$.)

The centre-to-centre spacing between successive vortical structures has been checked by flow visualization in the present flow to be $1{\cdot}75D$. On the other hand, the 'wavelength' was measured independently on the jet centre-line with the help of a lock-in amplifier, using the signal driving the loudspeaker as the reference. These measurements in the range $1 < x/D < 3$ yielded a (linear) variation of the phase of the fundamental ($\Delta\phi/\Delta x$) of 63°/inch. This gives a wavelength of $2{\cdot}25D$, agreeing quite well with the corresponding value inferred from the educed vorticity contours in figure 8.

As a matter of fact, one can clearly see that the measured wavelength should gradually decrease from the jet axis to the shear layer, being bounded between the two dotted lines through the vortex centres (figure 8). For the phase under study, $\langle u \rangle$ has maxima on these dotted lines. Under the excitation, the fundamental frequency of the periodic waveform remains constant everywhere in the flow field. This is apparent from the $\tilde{u}$-spectra anywhere on an (x, y) plane – the fundamental spectral spike does not shift in frequency. Thus, the above wavelengths should correspond to a longitudinal convection velocity of $0{\cdot}72U_e$ on the jet centre-line and $0{\cdot}53U_e$ in the middle of the shear layer. These values agree excellently with those obtained by Hussain & Clark (1981) for the most dominant structure in a natural axisymmetric shear layer, determined via the method of double-Fourier transformation of the space–time correlation of $\tilde{u}(t)$. These data thus clearly show that the changes in the orientation (or tilting) of the individual structures, as they travel downstream, can satisfactorily explain the variation of convection velocity across a shear layer, also observed by other investigators (Hussain & Clark 1981; Lau 1979). This may also be the reason why different values of the convection velocity in the near field of the jet have been reported.

(*d*) *Phase-average turbulence intensities and Reynolds stress.* The spatial distribution of the phase-average longitudinal turbulence intensity of the background random field ($\langle u_r^2 \rangle^{\frac{1}{2}}$), for the phase corresponding to figure 8, is shown in figure 9. The corresponding transverse intensity field ($\langle v_r^2 \rangle^{\frac{1}{2}}$) is shown in figure 10. In both figures, the vortex centres are marked by the $\oplus$ signs, and the dotted lines from the vortex centres to the jet centre-line (denoting spatial locations where $\langle u \rangle$ has maxima corresponding to the particular phase) are the same as those in figure 8. It is clear from figures 9 and 10 that maxima of $\langle u_r^2 \rangle^{\frac{1}{2}}$ and $\langle v_r^2 \rangle^{\frac{1}{2}}$ distributions occur near the vortex centres. Note that the locations of peak $\langle u_r^2 \rangle^{\frac{1}{2}}$ occur downstream of the peak $\langle u \rangle$ locations, where the fluid undergoes deceleration. These trends are consistent with those found for the single vortical structures in II.

The loss of periodicity in the passage of the coherent structure, downstream of the potential core, is further demonstrated by the distribution of the coherent structure Reynolds stress $\langle u_p v_p \rangle$ shown in figure 11 (note the expanded scales compared with figures 8–10). Alternate positive and negative $\langle u_p v_p \rangle$ with large amplitudes are encountered in the upstream locations where the vortex is strong (with high core peak

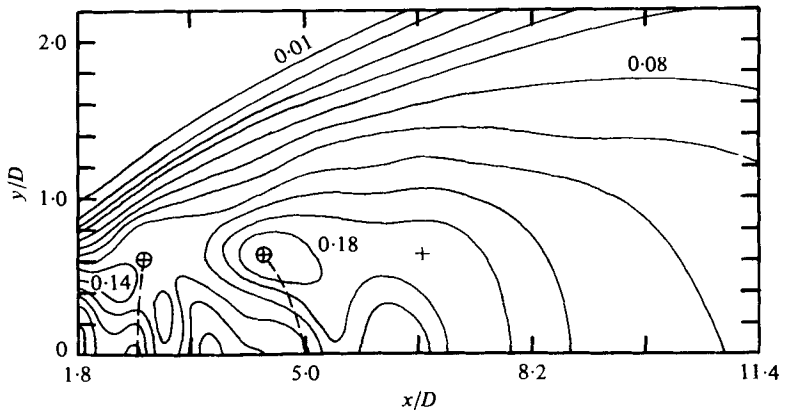

FIGURE 9. Contours of phase-average longitudinal turbulence intensity $\langle u_r^2\rangle^{\frac{1}{2}}/U_e$ corresponding to the phase and flow in figure 8. Contour levels in sequence are 0·01, 0·02, 0·03, 0·04, 0·06, 0·08, 0·10, 0·12, 0·14, 0·16, 0·18.

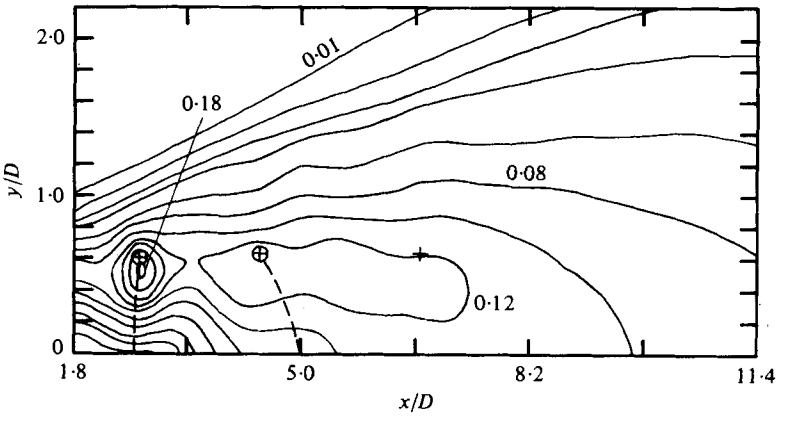

FIGURE 10. Contours of phase-average transverse turbulence intensity $\langle v_r^2\rangle^{\frac{1}{2}}/U_e$ corresponding to the phase and flow in figure 8 (same contour sequence as in figure 9).

vorticity). But farther downstream, the positive $\langle u_p v_p\rangle$ regions fast diminish in area while the negative $\langle u_p v_p\rangle$ regions persist somewhat. At around $x/D = 6{\cdot}5$, the absolute values of $\langle u_p v_p\rangle$ are in the measurement noise level, implying almost complete loss of the periodicity in the motion of the large-scale structures as well as increasing jitter with increasing x. Note that the tilt in the $\langle u_p v_p\rangle$ contours in the downstream regions is consistent with the tilt in the coherent vortices in those regions.

The background turbulence Reynolds stress $\langle u_r v_r\rangle$ corresponding to the data of figure 8 are presented in figure 12. Around a vortex centre (marked by the plus signs), $\langle u_r v_r\rangle$ contours are expected to have a minimax or a 'saddle point'; for an analytical discussion on this, see II. The vortex centres are approximately located at these saddle points (see later for more detailed data). Note that farther downstream (say, for $x/D > 7$), the $\langle u_r v_r\rangle$ variations are not significantly different from the $\overline{uv}$ variations as shown in figure 6(*b*).

A question naturally arises about how much of the intensities $\langle u_r^2\rangle^{\frac{1}{2}}$, $\langle v_r^2\rangle^{\frac{1}{2}}$ as well as $\langle u_r v_r\rangle$ are influenced by jitter. Examination of the contours of $\langle u_r^2\rangle^{\frac{1}{2}}$, $\langle v_r^2\rangle^{\frac{1}{2}}$

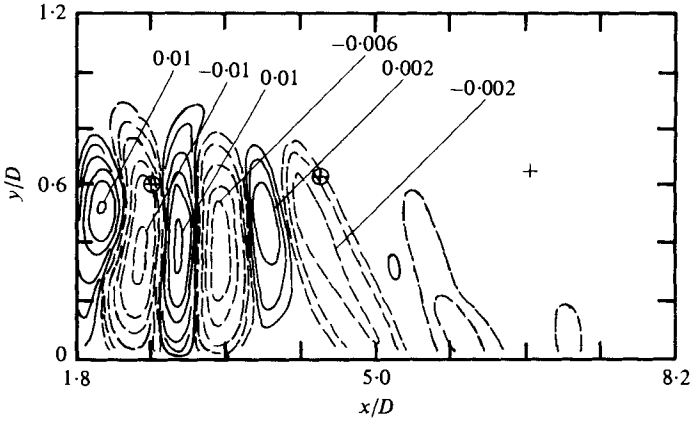

FIGURE 11. Contours of phase-average coherent Reynolds stress $\langle u_p v_p \rangle / U_e^2$ corresponding to the phase and flow in figure 8. Solid lines are for positive $\langle u_p v_p \rangle$, dashed lines are for negative $\langle u_p v_p \rangle$. Contour levels in sequence are −0·0005, −0·001, −0·002, −0·003, −0·004, −0·006, −0·01, and 0·0005, 0·001, 0·002, 0·003, 0·004, 0·006, 0·010.

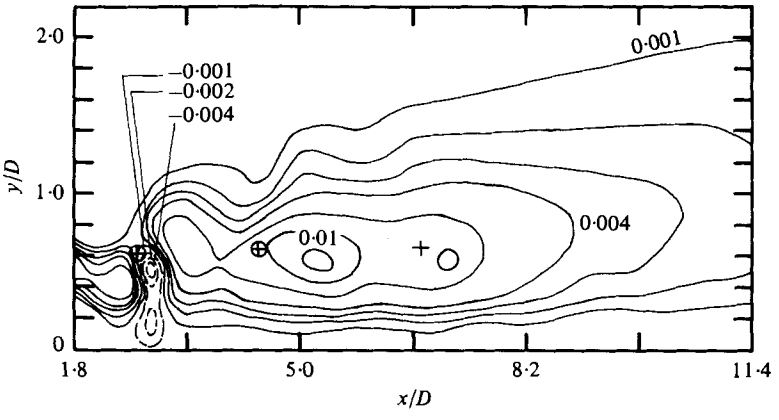

FIGURE 12. Contours of phase-average background turbulence Reynolds stress $\langle u_r v_r \rangle / U_e^2$ corresponding to the phase and flow in figure 8. Unmarked contour levels in sequence are 0·002, 0·003, 0·006, 0·008.

reveals that their peaks do not occur at the locations of maximum gradients of the corresponding phase-average values (i.e.of $\langle u_p \rangle$ and $\langle v_p \rangle$). Thus, $\langle u_r^2 \rangle^{\frac{1}{2}}$ and $\langle v_r^2 \rangle^{\frac{1}{2}}$ are not significantly influenced by jitter, and $\langle u_r v_r \rangle$ data truly represent the phase-average background turbulence Reynolds stress.

3.3. *Further characteristics of the coherent structure and its identification*

The detailed description of the instantaneous features of a single coherent structure and its geometry is of major interest because these features must constitute the building blocks for the development of an appropriate theory of turbulent shear flows based on coherent structure dynamics. Because the preferred mode is the most dominant and frequently occurring structure in an unperturbed jet, presumably an appropriate superposition of the corresponding coherent structures with random phases and sizes can lead to a viable theory for the circular jet flow. With this in mind,

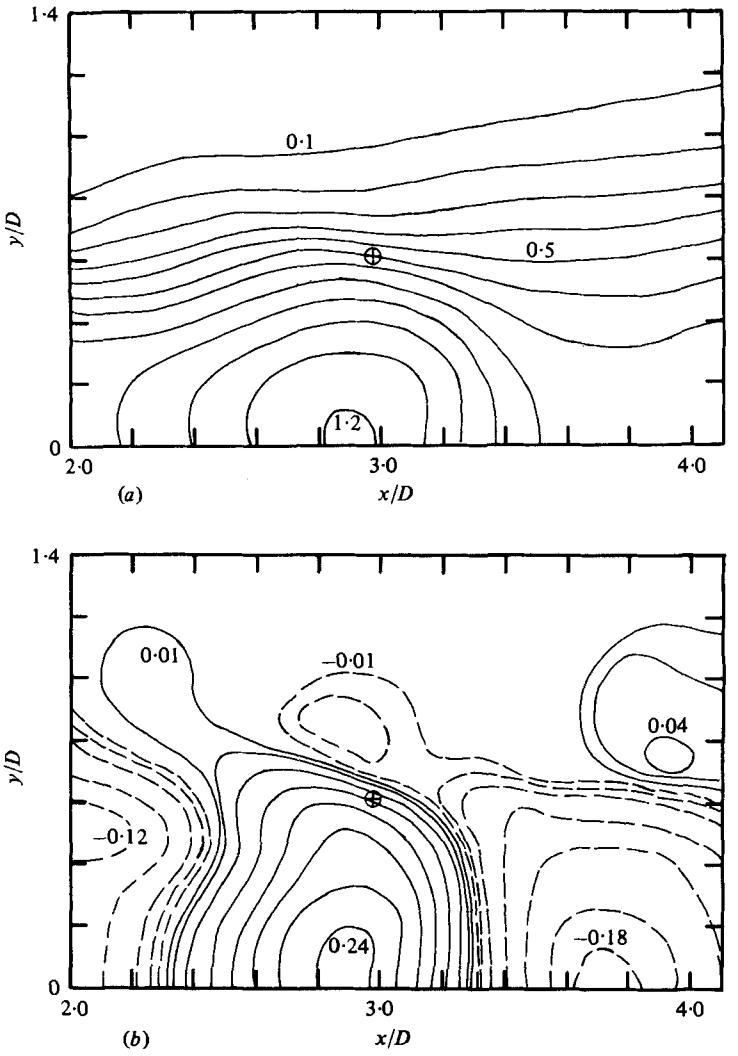

FIGURE 13. Phase-average velocity contours corresponding to the phase and flow in figure 7 (*d*). (*a*) $\langle u\rangle/U_e$; contour levels in sequence are 0·1, 0·2, 0·3, 0·4, 0·5, 0·6, 0·7, 0·8, 0·9, 1·0, 1·1 and 1·2. (*b*) $\langle u_p\rangle/U_e$; contour levels (dashed lines for negative and solid lines for positive) in sequence are −0·01, −0·02, −0·04, −0·08, −0·12, −0·16, −0·18, and +0·01, 0·02, 0·04, 0·08, 0·12, 0·16, 0·20, 0·24. (*c*) $\langle v_p\rangle/U_e$; contour levels in sequence are −0·01, −0·02, −0·04, −0·08, −0·12, and +0·01, 0·02, 0·04, 0·08; 0·12, 0·16.

further details of the preferred-mode structure are discussed in this section for one particular stage in the evolution of the structure, viz. that corresponding to the vorticity data in figure 7 (*d*), i.e. for $x_M/D \simeq 3$. Choice of this location was motivated by the considerations that it is sufficiently downstream from the jet lip so that the structure has fully matured, while it is sufficiently upstream from the end of the potential core so that breakdown of the structure has not commenced.

Contours of phase-average longitudinal velocity $\langle u\rangle$ are shown in figure 13 (*a*); the corresponding perturbation velocity field $\langle u_p\rangle (\equiv \langle u\rangle - U)$ representing the phase-average as a deviation from the local time-average velocity U is shown in figure 13 (*b*).

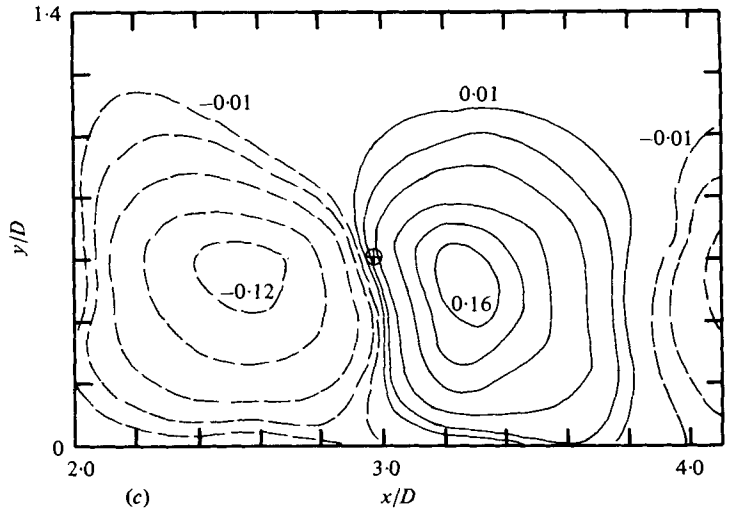

FIGURE 13(c). For legend see p. 58.

The corresponding $\langle v_p \rangle$ contours are shown in figure 13(*c*). Since V is relatively small, the contours of $\langle v \rangle$ are not radically different from those of $\langle v_p \rangle$ and are thus not shown. In the studies of the boundary-layer spot, contours of $\langle u_p \rangle / U_\infty = \pm 0{\cdot}02$ have been found to agree with the spot boundary and have been used as markers of the spot boundary (Coles & Barker 1975; Wygnanski *et al.* 1976; Zilberman *et al.* 1977). Comparison of contours in figures 13(*a–c*) with the vorticity contours in figure 7(*d*) and the streamlines and pseudo-stream-functions in figures 14(*a*, *b*) show that none of the contours of $\langle u \rangle$, $\langle u_p \rangle$ and $\langle v_p \rangle$ can serve to identify the boundary of the coherent structure in the jet. Note that, unlike the boundary-layer spot case, $\langle u_p \rangle$ contours are not even closed. The $\langle v_p \rangle$ contours show radially outward transport of the jet-core fluid at the front (downstream end) and radially inward transport of the ambient fluid at the back (upstream end) of the structure; the outward transport being larger than inward transport.

The spatial distribution of the phase-average velocity vector $(\langle u \rangle, \langle v \rangle)$ are plotted in figure 14(*a*); the dots indicate the origins of the vectors. Lines drawn tangential through these vectors would give the phase-average streamlines ψ_p associated with the coherent structure at the selected phase. Figure 14(*b*) shows contours of the pseudo-stream-function $\langle \psi \rangle = \int_0^y r(\langle u \rangle - U_{\text{ref}})\, dr / D^2 U_e$. Both figures 14(*a*) and 14(*b*) have been drawn with respect to a reference frame velocity $U_{\text{ref}} = 0{\cdot}55 U_e$, which is the approximate convection velocity of the structure. Note the close similarity between ψ_p and $\langle \psi \rangle$ even though the latter is derived from $\langle u \rangle$ data only. Thus, single-wire data may be adequate for inferring the cross-sectional shape of a (axisymmetric) coherent structure, a point emphasized in II. Comparison with the vorticity contour (figure 7*d*) shows that either of ψ_p or $\langle \psi \rangle$ satisfactorily identifies the overall shape and size of the coherent structure. The structure shape, as revealed in figure 14(*a*), with an aspect ratio of about 2:1, appears in close agreement with that educed by Yule (1978) in an unperturbed jet. In the scheme employed by Yule, the educed coherent structure is an average of natural structures of varying characteristics. The contours

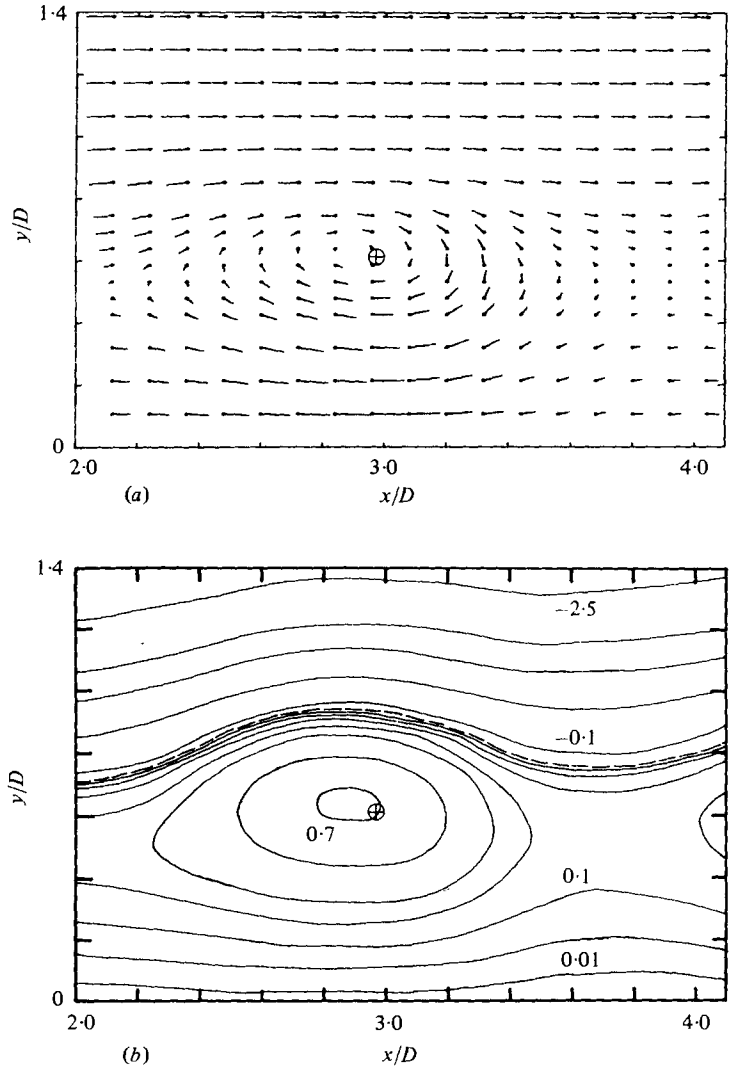

FIGURE 14. Phase-average streamlines ψ_p and contours of pseudo-stream-function $\langle\psi\rangle$ corresponding to the phase and flow in figure 7 (*d*), using a reference frame velocity of $U_{\text{ref}} = 0{\cdot}55U_e$. (*a*) ψ_p (the velocity vector field). (*b*) $\langle\psi\rangle$. Contour levels (10 times $\langle\psi\rangle$) in sequence are 0·7, 0·5, 0·3, 0·2, 0·1, 0·04, 0·01, −0·01 (dashed), −0·1, −0·5, −1·0, −1·5 and −2·5.

of properties are clearly smeared out except that the shape is dominated by the dominant natural structure. The close agreement between the average structure shape educed by Yule and the preferred-mode structure educed by us is a strong indication that the excitation induces, not an artificial structure, but the natural structure corresponding to the preferred mode.

The phase-average background turbulence intensities, have also been used at times to determine the structure location and its boundaries (H. Fiedler, private communication). The contours of $\langle u_r^2\rangle^{\frac{1}{2}}$ and $\langle v_r^2\rangle^{\frac{1}{2}}$, corresponding to the data in figure 7 (*d*), are shown in figures 15 (*a*) and (*b*), respectively. It is clear that these two quantities can also identify the shape and boundary of a structure. It is interesting to note that

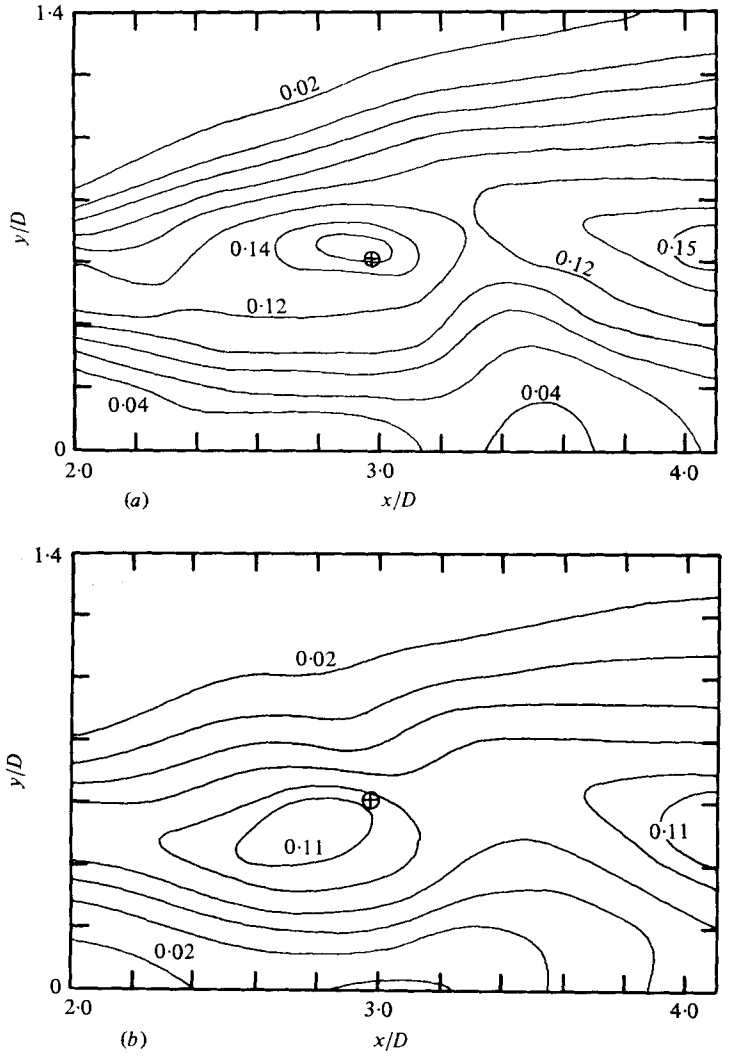

FIGURE 15. The phase-average turbulence intensities corresponding to the phase and flow in figure 7(*d*). (*a*) $\langle u_r^2\rangle^{\frac{1}{2}}/U_e$; (*b*) $\langle v_r^2\rangle^{\frac{1}{2}}/U_e$. The unmarked contour levels in sequence are 0·04, 0·06, 0·08, 0·10.

the peak of $\langle u_r^2\rangle^{\frac{1}{2}}$ occurs at the structure centre and $\langle v_r^2\rangle^{\frac{1}{2}}$ peak occurs slightly further upstream (discussed later). (Note that the structure centre is denoted by $\oplus$ in figures 13–15). One advantage of the contours of $\langle u_r^2\rangle^{\frac{1}{2}}$ and $\langle v_r^2\rangle^{\frac{1}{2}}$ over those of ψ_p and $\langle\psi\rangle$ is that the latter two are dependent on the reference frame convection velocity. Contours of ψ_p and $\langle\psi\rangle$ truly denote coherent structure shape and boundary only when plotted in a reference frame moving with the structure.

3.4. *The preferred-mode coherent structure at different Reynolds numbers and initial conditions*

How universal are the data reported in §§ 3.1–3.3? To what extent are the details of the preferred-mode coherent structure and its 'footprints' dependent on the jet size, speed, excitation frequency as well as the initial condition? Spatial distributions of

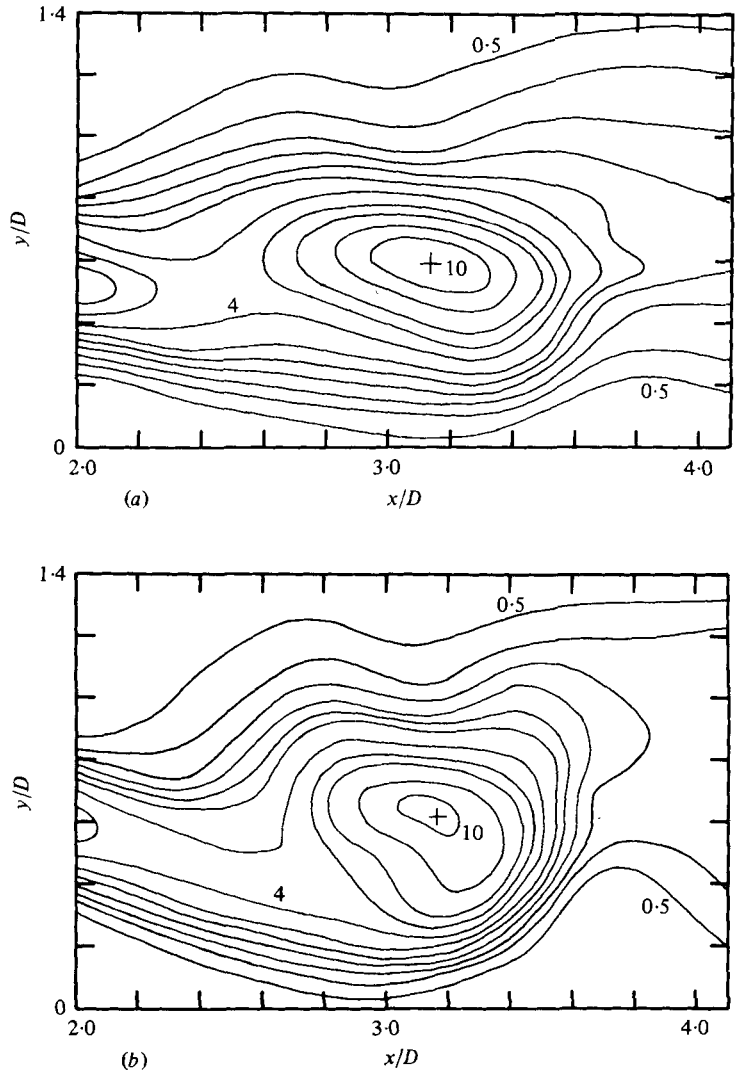

FIGURE 16. Contours of phase-average vorticity Ω_z/f_p for different Re_D and initial condition but all for excitation at $St_D = 0{\cdot}30$ with $u'_e/U_e = 2\,\%$. The phase for each case was chosen such that the structure would be centred at $x/D \simeq 3$. (*a*) Laminar initial boundary layer. All other flow parameters same as in figure 7(*d*) ($Re_D = 55000$ in the 7·62 cm jet). (*b*) 7·62 cm (tripped) jet at $Re_D = 110000; f_p = 87$ Hz. (*c*) 2·54 cm (tripped) jet at $Re_D = 25000; f_p = 178$ Hz. (*d*) 2·54 cm (tripped) jet at $Re_D = 44000; f_p = 312$ Hz. Unmarked contour levels in (*a*)–(*d*) are in the sequence 8, 6, 5, 3, 2·5, 2, 1·5, 1.

the phase-average measures have been explored in an attempt to determine the effects of the initial condition and jet Reynolds number on the preferred-mode structure. The sensitivity to the initial condition has been documented for the two asymptotically limiting cases: laminar and fully turbulent exit boundary layers. Corresponding to the region and phase in figure 7(*d*), (i.e. for $x_M/D \simeq 3$), four different sets of vorticity contours are presented in figures 16(*a–d*), all for excitation at $St_D = 0{\cdot}30$. Figure 16(*a*) is for the same Re_D, f_p and u'_e/U_e as in figure 7(*d*), except that the exit boundary layer was laminar (inferred from the mean velocity and fluctuation

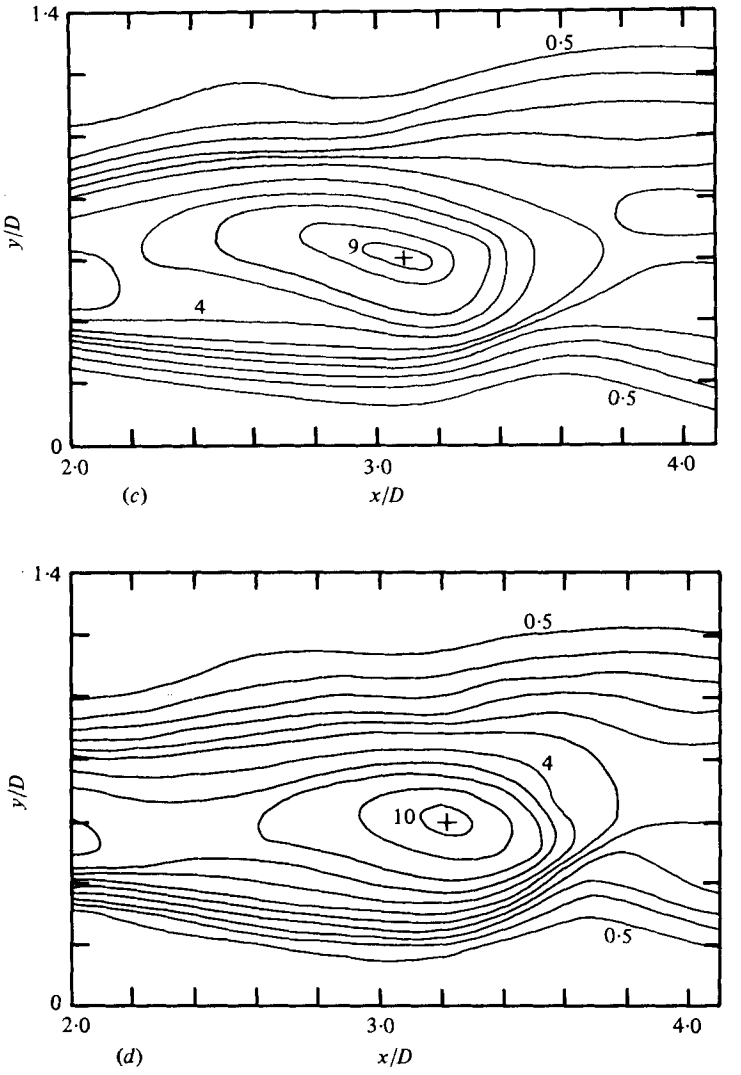

FIGURE 16(*c*, *d*). For legend see p. 62.

intensity profile characteristics and $\tilde{u}$-spectrum; for details see table 1 and also I). The data in figure 16 (*b*) represents a turbulent exit boundary-layer case in the 7·62 cm jet at a higher Re_D (= 110000). Figures 16 (*c*) and (*d*) are for the 2·54 cm tripped jet with Re_D values of 25000 and 44000, respectively. The characteristics of the initial boundary layers for the flows in figures 16 (*b–d*) are also listed in table 1. Note that the excitation frequency f_p for the Re_D = 44000 case is about 7 times that for the Re_D = 55000 case.

Comparison of figures 16 (*a*) with 7 (*d*) indicates that the structures in the region of measurement are essentially the same. The vortex centre in figure 16 (*a*), however, is slightly downstream from that in figure 7 (*d*). This is due to the uncertainty in the structure phase selection arising from jitter. Nevertheless, it is evident that the structure characteristics, viz. the aspect ratio, orientation and strength (indicated

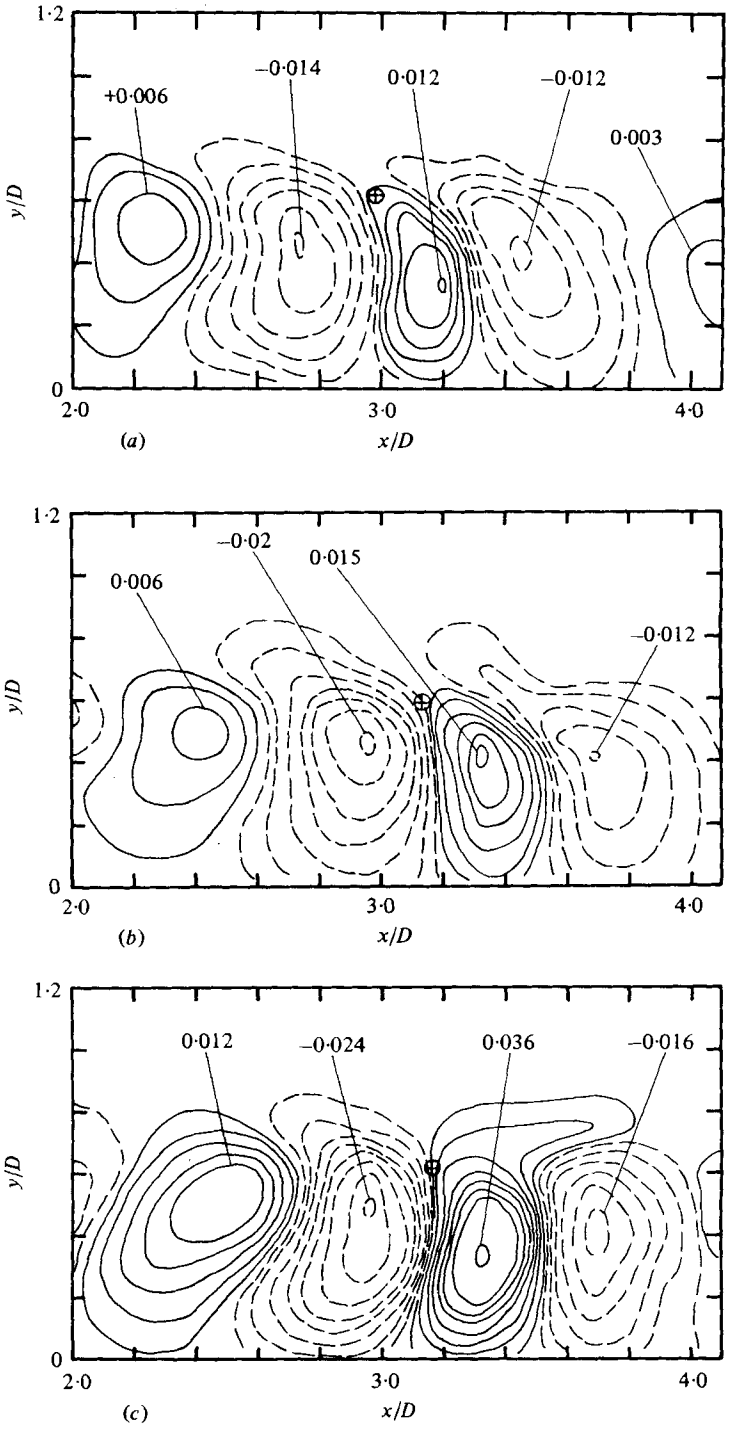

FIGURE 17. Contours of phase-average coherent Reynolds stress $\langle u_p v_p \rangle / U_e^2$. Data in (*a–d*) correspond to the flows in figures 7(*d*) and 16(*a–c*), respectively. Unmarked contour levels are in the sequence −0·016, −0·012, −0·009, −0·006, −0·003, −0·001, 0·001, 0·003, 0·006, 0·009, 0·012, 0·016.

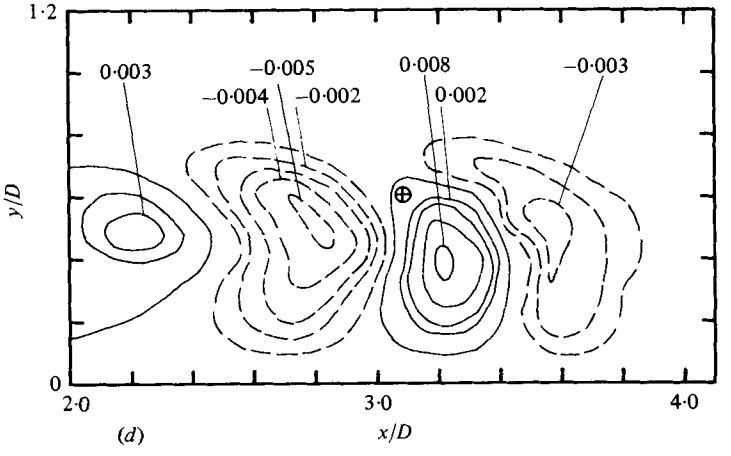

FIGURE 17(*d*). For legend see p. 64.

by peak vorticity), are essentially the same in the two flows. This is not unexpected in view of our observation in I based on the centre-line fluctuation intensity data that the circular-jet preferred mode occurs at $St_D \simeq 0{\cdot}30$, irrespective of the initial boundary layer being laminar or turbulent. The present data demonstrate for the first time that spatial features of the coherent structure for the jet-column preferred mode are independent of the initial boundary-layer characteristics.

However, the structure in figure 16(*b*), which is for excitation at $St_D = 0{\cdot}30$ but for a higher Reynolds number (110000) is somewhat different. Comparison with figure 7(*d*) or 16(*a*) shows that the structure aspect ratio and orientation are different but the normalized core vorticity levels are the same.

The effect of Re_D on the preferred-mode structure is further documented in figures 16(*a*) and (*d*) for the two lower Re_D's in the 2·54 cm (tripped) jet. Although the structures in these two figures are quite similar to those in figure 7(*d*) or 16(*a*), the differences in details, e.g. in the core size and aspect ratio should be apparent. Note that the normalized peak vorticity in the cores in all the figures 16(*a–d*) as well as figure 7(*d*) are the same; this is indeed striking since the excitation frequency for figure 16(*d*) is about 7 times that in figure 16(*a*). Thus, the dimensional peak vorticity in figure 16(*a*) is also 7 times that in figure 16(*a*). These data thus demonstrate that for the 'jet-column mode' structures (see I), the appropriate scaling factor for vorticity is the jet time scale D/U_e, irrespective of the jet exit speed, diameter or the initial condition.

Corresponding to the vorticity contours in figures 7(*d*) and 16(*a–d*), the contours of $\langle u_p \rangle$, $\langle v_p \rangle$, $\langle u_p v_p \rangle$, $\langle u_r v_r \rangle$, $\langle u_r^2 \rangle^{\frac{1}{2}}$, $\langle v_r^2 \rangle^{\frac{1}{2}}$ and the streamlines and pseudo-stream-functions have been obtained. For brevity, only $\langle u_p v_p \rangle$ and $\langle u_r v_r \rangle$ will be discussed for four of the five cases. Corresponding to figures 7(*d*), 16(*a–c*), the contours of $\langle u_p v_p \rangle / U_e^2$ are shown in figures 17(*a–d*) and of $\langle u_r v_r \rangle / U_e^2$ in figures 18(*a–d*), respectively. Note that, in spite of the two distinctly different initial conditions, the largely different Re_D and two jet sizes, there is close similarity among the contours of the coherent Reynolds stress $\langle u_p v_p \rangle$. With respect to the structure centre, marked by the $\oplus$ sign, the structure transports core fluid outwards at its front and outer ambient fluid inwards at its back. Note that the periodicity in x of the $\langle u_p v_p \rangle$ contours is

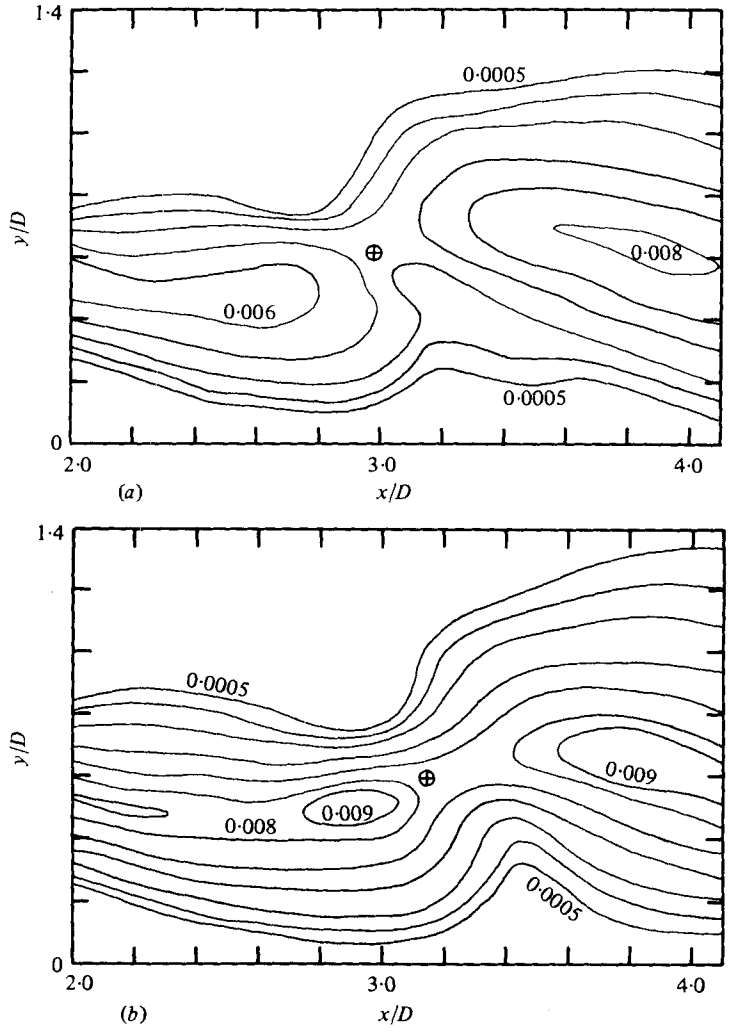

FIGURE 18. Contours of phase-average background turbulence Reynolds stress $\langle u_r v_r \rangle / U_e^2$. Data in (*a–d*) correspond to the flows in figures 7(*d*) and 16(*a–c*), respectively. Contour levels in sequence are 0·0005, 0·001, 0·002, 0·004, 0·006, 0·008.

twice that of the coherent structure, which is to be expected because $\langle u_p v_p \rangle$ is the result of the product of two periodic components $\langle u_p \rangle$ and $\langle v_p \rangle$ (see II).

The contours of the background turbulence Reynolds stress $\langle u_r v_r \rangle / U_e^2$ in figures 18(*a*)–(*d*) show that these are essentially identical for the two initial conditions. With increasing Re_D, the contours become wider and the kink around the structure centre becomes stronger, consistent with the more rounded structure at higher Re_D. However, the peak values are the same for the four cases. It is impressive that, for each Re_D and initial condition, the structure peak vorticity is located at the saddle points of the corresponding $\langle u_r v_r \rangle$ contours. This was predicted in II and was shown to be the case for the situation of vortex pairing as well as for a spark-induced coherent structure in the axisymmetric mixing layer (Hussain, Kleis & Sokolov 1980).

The contours of $\langle u_r^2 \rangle^{\frac{1}{2}}$ and $\langle v_r^2 \rangle^{\frac{1}{2}}$ for the five cases under consideration are essentially

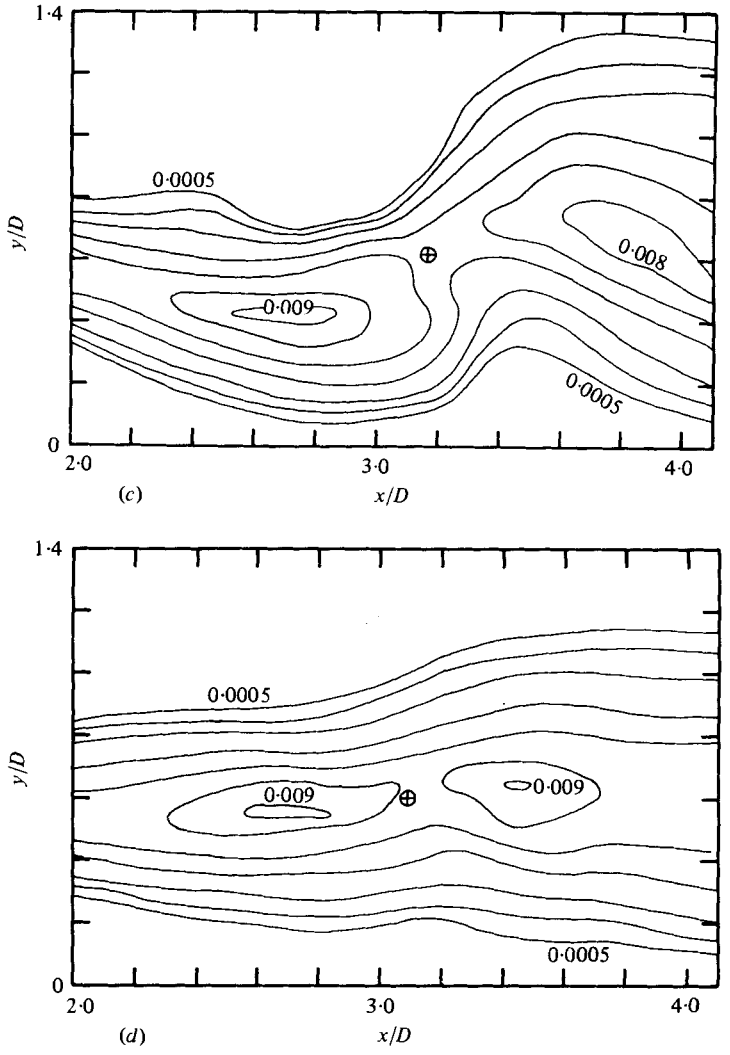

FIGURE 18(*c*, *d*). For legend see p. 66.

the same as those shown in figures 15(*a*, *b*) and are thus not shown. The maximum values of $\langle u_r^2 \rangle^{\frac{1}{2}}$ and $\langle v_r^2 \rangle^{\frac{1}{2}}$ are listed in table 2. The locations for peak values of $\langle u_r^2 \rangle^{\frac{1}{2}}$ and $\langle v_r^2 \rangle^{\frac{1}{2}}$ agree fairly with the structure centres identified by peak coherent vorticity.

Note that the background turbulence Reynolds stress is maximum in the braids which connect the centres of the structures. Contours of turbulence production (not presented) over the structure cross-section show that the production is large in the braids also. However, the coherent vorticity in the braid is low owing to continual advection of the braid fluid to the structure centres due to the structure-induced motion. Presumably, this motion deposits the turbulent braid fluid to the structure centres, which thus produces dilution of the core peak vorticity and simultaneously produces peak turbulence intensities at the structure centres. It should be mentioned that the 'dip' on the low-speed side of the vorticity contours, say in figures 16(*a–c*) are due to the combined effects of jitter and flow reversal, as was explained in II.

		Tripped			Laminar
$Re_D \times 10^{-3}$ ...		25	55	110	55
$\frac{\langle u_p v_p \rangle}{U_e^2}$		0·008 −0·005	0·012 −0·014	0·036 −0·024	0·016 −0·020
$\frac{\langle u_r v_r \rangle}{U_e^2}$	right left	0·009 0·009	0·008 0·007	0·009 0·009	0·010 0·010
$\frac{\Omega}{f_p}$		9·3	10·9	10·6	11·2
$\frac{\langle u_r^2 \rangle^{\frac{1}{2}}}{U_e}$		0·18	0·16	0·15	0·18
$\frac{\langle v_r^2 \rangle^{\frac{1}{2}}}{U_e}$		0·12	0·12	0·13	0·14
$\frac{\langle u_p \rangle}{Ue}$		0·20	0·24	0·32	0·24
$\frac{\langle v_p \rangle}{U_e}$	max min	0·12 −0·08	0·16 −0·12	0·24 −0·16	0·16 −0·12

TABLE 2. Peak levels of different measures.

The relatively lesser 'dip' in the present case compared to those in the vorticity contours for the case of stable pairing reported in II is due to the fact that the effect of jitter in the present data is minimized, as trigger for each structure is obtained with a reference signal obtained in the same measurement region.

It is interesting to note that in spite of largely varying Re_D, and thus f_p, the preferred-mode coherent structure vorticity, at $x/D \simeq 3$, is essentially constant, being equal to $3{\cdot}0U_e/D$. The peak value of the phase-average background turbulence Reynolds stress $\langle u_r v_r \rangle$ is about $0{\cdot}008U_e^2$. The peak values of $\langle u_r^2 \rangle^{\frac{1}{2}}$ and $\langle v_r^2 \rangle^{\frac{1}{2}}$, which occur at the structure centres, are about $0{\cdot}16U_e$ and $0{\cdot}12U_e$, respectively. However, the coherent Reynolds stress peaks (both positive and negative) increase with Re_D. These peak levels are also listed in table 2. With increasing Re_D, the structure cross-section, which is elongated in the streamwise direction at lower Re_D, becomes more rounded so that it is more effective in radial momentum transport, i.e. in producing Reynolds stress. Note the large but systematic increases in both the positive and negative peaks in $\langle u_p v_p \rangle$ contours from $Re_D = 25000$ to $Re_D = 110000$. The difference between the positive and negative peaks also increases with Re_D. The data also show that the peak values of $\langle v_p \rangle$ occurring at the front of the structure increases progressively with increasing Re_D. Correspondingly, the negative peak values of $\langle v_p \rangle$ occurring on the trailing end of the structure decreases progressively with increasing Re_D. The positive and negative peak values in the $\langle u_p \rangle$ contours also show similar systematic dependence on Re_D. These clearly suggest that the coherent structure becomes progressively more energetic with increasing Reynolds number.

The increasing peak values of $\langle u_p v_p \rangle / U_e^2$ with increasing Re_D may suggest higher time-average total Reynolds stress $\overline{uv}/U_e^2$ at higher Re_D. While that may be so for an excited jet (at its preferred mode), clearly it cannot be the case for the unexcited jet because it will then violate the principle of Reynolds number similarity or asymptotic

invariance. (Even though there is no conclusive validation of this 'principle', asymptotic invariance is believed by most researchers to be true). This can probably be reconciled by the fact that, in an unexcited axisymmetric mixing layer, the coherent structures have been found to become less frequent with increasing Reynolds numbers (Hussain & Clark 1981). Thus, in an unexcited layer, although the Reynolds stress associated with the structures increases with Re_D, the total time-average, non-dimensional Reynolds stress is essentially independent of Re_D provided the latter is large enough.

4. Concluding remarks

Detailed distributions of different time-average and phase-average flow properties for an axisymmetric free jet under controlled perturbation at the jet preferred mode have been explored, and these data have been compared with the corresponding unexcited jet data. The effect of the perturbation is to increase jet spread and mean velocity decay as well as to increase the peak values of the time-average fluctuation intensities and Reynolds stress in the axisymmetric mixing layer. The changes brought about by the excitation in the time-average measures are significant, though not as dramatic as those for stable vortex pairing. This paper presents heretofore unexplored features of the preferred-mode coherent structure in the near field of the axisymmetric free jet. Controlled excitation has permitted documentation of the coherent structure properties to such detail as are unlikely to be possible in an unexcited jet even with the application of the most sophisticated detection schemes conceivable.

Coherent vortical structures with cores characterized by closed vorticity contours could be educed as far downstream as $x/D \simeq 6$. Closed vorticity contours are not observed for distances farther downstream. The spatial oscillations in the contours for $x/D > 6$, however, indicate some remnants of the periodic structure. These phase-average vorticity data, also supported by time-average $\tilde{u}$-spectra data, show that the periodicity in the passage of the coherent structures is lost beyond $x/D \simeq 8$, even though the structures are initially organized by the controlled excitation at the jet preferred mode. The phase-average data and also the $\tilde{u}$-spectra data clearly indicate total absence of any tendency for pairing of the preferred-mode coherent structure.

The transverse variation of the wavelength and convection velocity of the characteristic structures, observed in earlier investigations, are explained by the characteristic elongation and tilting of the structures as they travel downstream. Some time-average flow features in the excited jet could be qualitatively explained in terms of the sizes, shapes and strengths of the (educed) vortical structures.

Comparison of the contours of phase-average longitudinal and lateral velocities $\langle u_p \rangle$, $\langle v_p \rangle$ with the contours of coherent vorticity, streamlines and pseudo-stream-functions show that, unlike the boundary-layer spot, the contours of $\langle u_p \rangle$ or even $\langle v_p \rangle$ do not mark the boundary of the structure. The streamline pattern and the aspect ratio of the structure, when located at $x/D \simeq 3$, agree closely with those of the naturally occurring 'average' structure educed by Yule (1978). This, therefore, supports our contention that the controlled perturbation, rather than inducing an artificial structure, merely triggers the formation of the dominant natural (preferred-mode) structure. The transverse variation of wavelength and convection velocity measured by us across

the jet also agree with those measured for the dominant structure in the near field of an unperturbed jet.

It is shown that the preferred-mode coherent structure characteristics are independent of whether the initial shear layer is laminar or fully turbulent. The strength of the coherent structure as denoted by the core peak vorticity, non-dimensionalized by the preferred-mode frequency, is the same at different Reynolds numbers and initial conditions. However, the structure size and orientation have been found to depend somewhat on the Reynolds number. With increasing Re_D, the structure becomes shorter in the streamwise length and thicker in the radial extent. That is, it becomes progressively more rounded at higher Re_D and thus becomes more efficient in radial momentum transport, i.e. in the production of coherent Reynolds stress. The coherent velocities $\langle u_p \rangle$, $\langle v_p \rangle$ and the positive and negative peaks of the coherent Reynolds stress, as well as the difference between their absolute values, increase with Re_D. However, the total time-average Reynolds stress does not necessarily increase with Re_D, presumably because coherent structures occur less frequently with increasing Re_D. This dependence of the coherent structures on Re_D suggests that, for Reynolds number similarity to be achieved, Re_D should be much greater than what is commonly assumed. The present data indicate that the similarity has not been reached even at a Re_D value of 10^5. Thus one should guard against extrapolating to high-Reynolds-number jets the characteristics obtained with jets of Reynolds numbers significantly lower than 10^5.

Nearer to the jet exit, the coherent Reynolds stress is considerably larger than the background turbulence Reynolds stress, thus suggesting that the large-scale coherent structures are comparatively much more dominant than the fine-scale turbulence. However, the relative dominance is clear only in the early formation or pristine states of the structure. Our accumulated experience suggests that, with increasing distances farther downstream, the relative dominance of coherent structure decreases and becomes comparable to that of the background turbulence. Thus, the view held by some researchers that the large-scale coherent structures are dominant even in the fully developed states of the flow is unsubstantiated and appears unlikely; the contributions of the smaller-scale structures cannot be disregarded.

There is no evidence of pairing of the jet-column preferred-mode coherent structure. In an unperturbed jet, since the St_D corresponding to the most dominant structure is about 0·3 at $x/D \simeq 4$ – for both laminar and turbulent initial states – it would appear that there is no pairing activity farther downstream. However, since noise production in a jet mostly occurs near the end of the potential core (Bishop, Ffowcs Williams & Smith 1971; L. Maestrello, private communication), it seems that in an unperturbed jet it is not the pairing activity that plays the crucial role in noise production. The toroidal vortical structures formed upstream, break down farther downstream through the evolution of azimuthal lobe structures (I, II). Therefore, it appears that the formation of these lobes and the associated breakdown of the vortices, rather than the vortex-pairing event, is important in the production of aerodynamic noise in a jet.

We are thankful to Professor L. S. G. Kovasznay who made a careful review of the manuscript, a few weeks before his accidental death on 17 April 1980. This paper is dedicated to his memory. This research has been supported by the NASA Langley

Research Center under grant NSG-1475 and the National Science Foundation under grant ENG-7822110.

REFERENCES

Bechert, D. & Pfizenmaier, E. 1975 *J. Sound Vib.* **43**, 581.

Bishop, K. A., Ffowcs Williams, J. E. & Smith, W. 1971 *J. Fluid Mech.* **50**, 21.

Browand, F. K. & Laufer, J. 1975 *Turb. Liquids* **5**, 333. Univ. of Missouri-Rolla.

Browand, F. K. & Wiedman, P. D. 1976 *J. Fluid Mech.* **76**, 127.

Brunn, H. H. 1977 *J. Fluid Mech.* **83**, 641.

Cantwell, B., Coles, D. & Dimotakis, P. 1978 *J. Fluid Mech.* **87**, 641.

Chan, Y. Y. 1974 *Phys. Fluids* **17**, 1667.

Coles, D. & Barker, S. J. 1975 *Turbulent Mixing in Nonreactive and Reactive Flows* (ed. S. N. B. Murthy), p. 285. Plenum.

Crow, S. C. & Champagne, F. H. 1971 *J. Fluid Mech.* **48**, 547.

Hussain, A. K. M. F. & Clark, A. R. 1981 *J. Fluid Mech.* **104**, 263.

Hussain, A. K. M. F., Kleis, S. J. & Sokolov, M. 1980 *J. Fluid Mech.* **98**, 97.

Hussain, A. K. M. F. & Reynolds, W. C. 1970 *J. Fluid Mech.* **41**, 241.

Hussain, A. K. M. F. & Zaman, K. B. M. Q. 1980 *J. Fluid Mech.* **101**, 493.

Lau, J. C. 1979 *Proc. Roy. Soc.* A **368**, 547.

Michalke, A. 1972 *Prog. Aero. Sci.* **12**, 213.

Moore, C. J. 1977 *J. Fluid Mech.* **80**, 321.

Sokolov, M., Hussain, A. K. M. F., Kleis, S. J. & Husain, Z. D. 1980 *J. Fluid Mech.* **98**, 65.

Vlasov, Y. V. & Ginevskiy, A. S. 1974 *N.A.S.A.* TTF-15, 721.

Wygnanski, I., Sokolov, M. & Friedman, D. 1976 *J. Fluid Mech.* **78**, 785.

Yule, A. J. 1978 *J. Fluid Mech.* **89**, 413.

Zaman, K. B. M. Q. & Hussain, A. K. M. F. 1980 *J. Fluid Mech.* **101**, 449.

Zaman, K. B. M. Q. & Hussain, A. K. M. F. 1981 *J. Fluid. Mech.* **103**, 133.

Zilberman, M., Wygnanski, I. & Kaplan, R. E. 1977 *Phys. Fluids Suppl.* **20**, S258.